We are IntechOpen, the world's leading publisher of Open Access books
Built by scientists, for scientists

6,300
Open access books available

170,000
International authors and editors

185M
Downloads

154
Countries delivered to

Our authors are among the

TOP 1%
most cited scientists

12.2%
Contributors from top 500 universities

CLARIVATE ANALYTICS
BOOK CITATION INDEX
INDEXED

WEB OF SCIENCE™

Selection of our books indexed in the Book Citation Index
in Web of Science™ Core Collection (BKCI)

Interested in publishing with us?
Contact book.department@intechopen.com

Numbers displayed above are based on latest data collected.
For more information visit www.intechopen.com

Chapter

Magnetospheric Current Systems and the Polar Cap Index

Peter Stauning

Abstract

The transpolar convection of plasma and embedded magnetic fields generated by the solar wind interaction with the magnetosphere can be characterized by the polar cap (PC) indices, PCN (North) and PCS (South). These indices are derived from polar magnetic variations and calibrated with respect to the solar wind merging electric field (coupling function), E_M, considered to control the entry of solar wind energy into the magnetosphere providing power to disturbance processes such as magnetic storms, auroral substorms, and upper atmosphere heating. Thus, the PC indices could be used to quantify the solar wind intensities for solar-terrestrial research and to survey the entry of solar wind energy for space weather monitoring. The closest relations between PC indices and the geomagnetic disturbance processes are obtained by using the dual polar cap PCC indices built from the positive values of PCN and PCS. The present work demonstrates that the transpolar convection processes characterized by the PCC indices are closely related to the intensities of auroral electrojet currents, to substorm occurrences, and to the building of magnetospheric ring currents in the equatorial region at 4–6 earth radii distance.

Keywords: solar wind/magnetosphere interactions, polar cap index, auroral electrojet currents, magnetospheric ring currents, magnetic storms and substorms, space weather forecasting.

1. Introduction

The magnetosphere comprises a number of current systems contained within the geomagnetic bubble carved out in the solar wind flow of tenuous ionized gasses flowing from the solar surface carrying solar magnetic fields out into space.

Dungey [1] formulated the concept of magnetic merging processes taking place at the front of the magnetosphere between the interplanetary magnetic field (IMF), when southward oriented, and the geomagnetic field, followed by the draping of the combined solar and geomagnetic fields and associated ionized plasma over the poles creating an elongated magnetospheric structure. In the extended magnetospheric tail region, the geomagnetic field from the northern and southern hemisphere would reconnect releasing the solar magnetic fields. The restored geomagnetic field would then be convected sunward at lower latitudes to resume merging with the solar wind field at the front of the magnetosphere.

The high-latitude antisunward ionospheric and magnetospheric plasma drift across the polar cap (PC) and the return flow in the sunward motion along dawn and dusk auroral latitudes generate the two-cell "forward convection" patterns, later termed DP2 (Polar Disturbance type 2) by Obayashi [2], Nishida [3], and Nishida and Maezawa [4]. Subsequently, Dungey [5] extended his model to include cases where IMF is northward (NBZ conditions), which in stronger cases would reverse the convection patterns in the central polar cap and generate sunward transpolar "reverse convection" plasma flow later termed DP3 (Polar Disturbance type 3) possibly inside a residual two-cell forward convection system. Although many details have been added later [6], these solar wind-magnetosphere interaction models still prevail now, 60 years later. The strictly southward or northward IMF directions in the idealized models have been extended to all IMF directions while retaining the basic features of northward versus southward IMF orientation.

In addition to the magnetopause currents (MPC) marking the interface between the solar wind and geomagnetic space, the magnetosphere comprises the polar cap transpolar currents and the auroral current systems both intimately connected to the plasma convection, the tail current sheet connecting the magnetopause flanks, and the ring currents of ions encircling the Earth at middle, low, and equatorial latitudes at distances of 4–6 earth radii. It is the primary objective of the present contribution to demonstrate that these magnetospheric current systems are closely interrelated in terms of the polar cap (PC) indices, notably the dual polar cap PCC indices.

The polar cap indices, PCN (North) and PCS (South), based on magnetic data recorded at the central polar cap observatories in Qaanaaq (Thule) in Greenland and Vostok in Antarctica, respectively, were developed from the initial concept by Fairfield [7] through the pioneering works of Kuznetsov and Troshichev [8], Troshichev and Andrezen [9], and Troshichev et al. [10]. Further PC index developments were made by Vennerstrøm [11], Troshichev et al. [12, 13], Stauning et al. [14], and Stauning [15–20].

To derive PC index values, magnetic variations related to the transpolar convection of plasma and magnetic fields are calibrated against the values of the merging electric field (coupling function), E_M (=E_{KL}, [21]), derived from parameters in the impinging solar wind. The calibration parameters are based on the statistical processing of solar wind and geomagnetic data throughout an epoch of accumulated values. Through their association with E_M, the PC indices represent the merging processes between the solar wind magnetic fields extending from the Sun and the terrestrial magnetic fields at the magnetospheric boundaries and could be considered representative of the energy transfer from the solar wind to the magnetosphere. This energy may be temporarily stored in the magnetospheric tail configuration to be dissipated in processes such as auroral substorms, upper atmosphere heating, and ring current enhancements. In further developments, interactions between the solar wind and polar cap convection processes include the effects of the related field-aligned current systems and also the consideration of reconnection processes at the nightside [22].

Janzhura et al. [23] have used the PC indices in substorm studies to predict the duration of the growth phase at substorm developments. For isolated events, they estimated that substorm onset would occur as the PC index level reached ∼2 mV/m. From the investigations of a large number of substorms, Troshichev et al. [24] concluded that substorm onset was likely to happen when the PC index starting from a low level exceeded 1.5 ± 0.5 mV/m.

Troshichev et al. [25] and Troshichev and Sormakov [26] have used PC indices to predict the maximum intensities (SYM-H minima) during geomagnetic storms. In the studies of geomagnetic storms by Stauning et al. [27] and Stauning [28, 29], the PC indices have been implemented in gradient source functions used to predict the development of ring current intensities characterized by Dst index values.

Among important applications of real-time PC indices are forecasts of strong substorms that may threaten power grids through their geomagnetically induced current (GIC) effects [30, 31]. An investigation of GIC-related high-voltage power line disturbances in Scandinavia [32] has demonstrated that the PC index values most often would remain at a high level for more than 2–3 h up to reported major power line cuts. The lengthy pre-event intervals, which are also reflected in the ring current indices [29], are most likely needed for enabling the merging processes at the front of the magnetosphere and subsequent transpolar convection characterized by the PC indices to load the tail configuration with enough energy to generate violent substorm events. The enhanced merging processes during extended pre-event intervals make the polar cap expand to enable substorm activity reaching subauroral latitudes, where important power grids reside. According to these investigations, PC index levels above ~10 mV/m maintained throughout more than 1 h should cause alert for subauroral power grids [32, 33].

Strong auroral currents in the polar ionosphere characterized by large PC index values may cause heating of the upper atmosphere, which would then expand to cause anomalies in satellite orbits. The ring current intensities characterized by the Dst indices, which are related to PC index values, have been associated with further space weather effects such as spacecraft charging. The resulting electrostatic discharges in spacecraft structures may cause harmful anomalies in satellite electronic systems [34].

The report ISO/TR23989:2020 [35] issued by the authoritative Technical Committee of the International Organization for Standardization (ISO) for the natural and artificial space environment discusses the operational estimation of the solar wind energy input into the Earth's magnetosphere. The report aims at providing guidelines for the use of operative ground-based information on the polar cap magnetic activity defined by the PC indices. The report notes: "*The solar wind energy incoming into the magnetosphere predetermines development of the magnetospheric disturbances: magnetic storms and substorms. Magnetospheric disturbances include a wide range of phenomena and processes directly affecting human activity, such as satellite damage, radiation hazards for astronauts and airline passengers, telecommunication problems, outages of power and electronic systems, effects in the atmospheric processes, and impact on human health.*"

2. The polar cap (PC) index concept

The main purpose of the polar cap (PC) index concept is formulating a parameter that would quantify the transfer of energy from the solar wind to the magnetosphere to generate global geomagnetic disturbances such as magnetic storms and substorms. This makes the PC index fundamentally different from the auroral electrojet (AE) indices and further ground based magnetic indices such as the planetary disturbance index (Kp), and the ring current indices (Dst, SYM, and ASY), which represent the dissipation of the energy received from the solar wind. In the initial version by Troshichev and Andrezen [9], the polar cap index was derived directly from polar magnetic variations. However, this index type depends critically on daily and seasonal variations in ionospheric conductivities.

A major progress in the development of the PC index concept came with the work of Troshichev et al. [10] introducing the scaling of polar magnetic variations against the so-called merging or geoeffective electric fields in the formulation by Kan and Lee [21]. This energy coupling function is actually based on a theoretical concept using a particular projection of the electric field assumed to relate to the interface between two colliding magnetized plasma bodies. The merging electric field function holds the important solar wind parameters, the velocity, V_{SW}, and the interplanetary magnetic field (IMF) strength and orientation in the geocentric solar magnetospheric (GSM) representation. The energy coupling concept was initially developed by Akasofu [36–38] to provide the so-called epsilon (ε) parameter considered to be of major relevance for substorm developments and then modified by Kan and Lee [21] to provide a convenient relation between important solar wind parameters and the supply of energy to geomagnetic disturbances.

With the new PC index concept, the solar wind parameters (V_{SW} and IMF GSM-B_Y, GSM-B_Z) are replaced by polar cap horizontal magnetic variations (ΔF_H), which relate to polar current systems (horizontal and/or field-aligned) generated by the solar wind-magnetosphere interactions and measurable from ground. Thus, the estimates of solar wind energy input could be based on reliable and continuous ground-based observations. Furthermore, with the scaling against parameters in the solar wind, the new index would be independent (in principle) of local conditions such as variable ionospheric conductivities and observatory position within the polar caps.

3. Derivation of PC index values

The descriptions of the steps in the calculations of PC indices can be found elsewhere, for instance, in Troshichev et al. [12–14] or Stauning [17–20]. They are summarized here for convenience. The polar magnetic disturbance vector is defined by

$$\Delta \boldsymbol{F} = \boldsymbol{F} - \boldsymbol{F}_{RL} \tag{1}$$

where the reference level, $\boldsymbol{F}_{RL}$, is composed of the secularly varying component, $\boldsymbol{F}_{BL}$, and a daily varying term, $\boldsymbol{F}_{QDC}$, the quiet day curve (QDC), representing the daily magnetic variation during quiet conditions. Thus

$$\Delta \boldsymbol{F} = \boldsymbol{F} - \boldsymbol{F}_{BL} - \boldsymbol{F}_{QDC} \tag{2}$$

In order to focus on solar wind effects and reduce the influence from currents associated with localized features, such as density gradients, the horizontal magnetic variations, $\Delta \boldsymbol{F}$, of the recorded horizontal magnetic field vector series are projected to an "optimum direction" in space to provide the scalar projected variations, ΔF_{PROJ}.

The optimum direction is assumed to be perpendicular to the DP2 transpolar convection-related sunward equivalent currents and characterized by its varying angle, φ, with the dawn-dusk meridian.

The solar wind energy coupling function, E_{KL}, here named "merging electric field," E_M, because of its inherent dimension (mV/m) is defined as follows [21]:

$$E_M = V_{SW} \left(B_Y{}^2 + B_Z{}^2 \right)^{\frac{1}{2}} \sin^2(\theta/2) : \theta = \arctan(B_Y/B_Z) \tag{3}$$

where V_{SW} is the solar wind velocity, B_Y and B_Z are the GSM components of the interplanetary magnetic field (IMF), and θ is the polar angle of the transverse IMF vector. In consequence of its role as an energy coupling function, the projected polar cap magnetic disturbances, ΔF_{PROJ}, are assumed being proportional to E_M:

$$\Delta F_{PROJ} = \alpha E_M + \beta \tag{4}$$

where α is the slope and β is the intercept parameter named from a graphical display of the relation between ΔF_{PROJ} and E_M.

The polar cap (PC) index is now defined by equivalence with E_M in the inverse relation of Eq. (4), i.e.,

$$PC = (\Delta F_{PROJ} - \beta)/\alpha : (\approx E_M) \tag{5}$$

With the relation in Eq. (5), the ΔF_{PROJ} scalar values are scaled to make the PC index equal (on the average) to values of E_M in the solar wind. The scaling of the polar cap magnetic disturbances to a quantity in the solar wind removes (in principle) the dependence on the daily and seasonally varying ionospheric conductivities and other local conditions, such as the location of the measuring polar magnetic observatory.

The projection angle for the projection of the horizontal magnetic variation vector in its geographic representation, $(\Delta F_X, \Delta F_Y)$, in the (rotating) observatory frame at longitude, λ, to the optimum direction, φ, in space is defined by

$$V_{PROJ} = \text{Longitude} (\lambda) + \text{UTh} \cdot 15° + \text{optimum direction angle} (\varphi) \tag{6}$$

where UTh is the UT time at the observatory in hours.

Thus, the projected magnetic variations could be expressed by

$$\Delta F_{PROJ} = \Delta F_X \cdot \sin(V_{PROJ}) \pm \Delta F_Y \cdot \cos(V_{PROJ}) : (+\text{for southern}, -\text{for northern hemisphere}) \tag{7}$$

The propagation delay, τ, between parameters at the reference location in space for the solar wind data and the location for related effects at the polar cap, and the values of the optimum angle, φ, are both estimated from searching optimum correlation between E_M and ΔF_{PROJ} [12–14, 17]. The correlation coefficient is usually around R = 0.75, while the delay from the magnetospheric bow shock nose (BSN) to recorded effects in the polar cap is close to τ = 20 min regardless of the rotating observatory positions within the magnetospheric polar cap. The delay varies little with seasonal and solar activity conditions.

The calibration parameters, the slope, α, and the intercept, β, are estimated for each moment of the day and year by linear regression between time-delay-adjusted samples of ΔF_{PROJ} and E_M using past data from an extended epoch, preferably a complete solar cycle [12–14, 17]. The regression parameters and the optimum angle values are usually derived as hourly values but interpolated and tabulated throughout the year at 1-min resolution. They are kept invariant over years unless a new index version is introduced.

Forward convection (DP2) patterns prevail during conditions, where the IMF B_Z component is negative or just small, and generate positive ΔF_{PROJ} values. The slope parameter (α) is positive and the intercept term (β) is relatively small. Hence, the PC index values, according to Eq. (5), are mostly positive. During positive (northward)

and strong IMF B_Z (NBZ) conditions, reverse convection patterns (DP3) may emerge and generate negative ΔF_{PROJ} values, which, in turn, may generate negative PC index values.

The PCC (PC combined) indices are derived from the means of non-negative values of the PCN and PCS indices filling zeroes for negative index values [15]:

$$PCC = (PCN \text{ if} > 0 \text{ or else } 0 + PCS \text{ if} > 0 \text{ or else } 0)/2. \qquad (8)$$

Thus, the PCC index values are always non-negative like the merging electric field, E_M, used for the calibration of the individual polar cap indices. At negative PC index values in both the hemispheres, the global magnetic activity goes low like the PCC index values. However, there could still be local magnetic activity such as upper atmosphere auroral heating and reverse transpolar ionospheric convection. Positive PC index values in one hemisphere indicates unipolar solar wind energy entry and the generation of global magnetic disturbances in agreement with the positive PCC index levels even if the PC index for the other hemisphere is dominatingly negative and would generate negative PC index values by simple averaging of PCN and PCS values. Even at lengthy intervals of negative PCN and PCS values, the magnetosphere is not emptied of energy but usually enters a low-activity state.

4. Basic polar magnetic observations

The magnetic data used for the standard PCN indices are collected from Qaanaaq (THL) observatory in Greenland operated by the Danish Meteorological Institute (DMI), while the Danish Space Research Institute (DTU Space) operates the magnetic instruments and takes care of the data collection and processing. Data for the standard PCS indices are collected from the Antarctic Vostok observatory operated by the Arctic and Antarctic Research Institute (AARI) in St. Petersburg, while data for an alternative PCS index are collected at the French-Italian Dome Concordia (Dome-C) observatory [39, 40]. An alternative source for the PCN index is Alert observatory in Canada operated by the Canadian Energy and Mining administration. The characteristics of the four locations, including essential geomagnetic parameters based on the NASA VITMO application for 2021, are specified in **Table 1**.

Prior to their use in PC index calculations, the magnetic data are carefully examined. It is of major importance that the base-level values are correctly adjusted. As one of the important measures used to disclose possible problems, the monthly average X- and Y-component values are inspected. These values are derived as the means of measured values for all hours of the 5 quietest (QQ) days each month. These dates are

Observatory	Station	Latitude	Longitude	CGMlat	CGMlon	LT = 00	MLT = 00
Name	Acr.	Deg.	Deg.	Deg.	Deg.	UThrs	UThrs
Qaanaaq	THL	77.47	290.77	83.86	23.86	4.62	3.60
Alert	ALE	82.50	297.65	87.02	70.10	4.16	0.14
Dome-C	DMC	–75.25	124.17	–89.31	44.52	15.72	1.77
Vostok	VOS	–78.46	106.84	–84.04	56.64	16.88	0.95

Table 1.
Geographic and geomagnetic parameters at 100 km of altitude for selected stations.

defined by the International Service for Geomagnetic Indices (ISGI) available at
http://isgi.unistra.fr. **Figure 1a** and **b** display the average values for the observed X
and Y components from Qaanaaq (THL) and Vostok (VOS).

The average X- and Y-component values for Qaanaaq (THL) display smooth
secular changes that are easily interpolated to create adequate baseline values
throughout the displayed years. It is evident from **Figure 1b** that the definition of
proper baseline values for Vostok presents challenges by the irregular variations and
unexpected jumps. The base levels need comprehensive adjustments to remove irregu-
lar base-level changes and retain smooth secular variations only. Such adjustments
are described (to some length) in [17].

The next step in the processing of the polar magnetic data is deriving the quiet
daily variations, the quiet day curve (QDC), for each of the two horizontal vector

(a)

(b)
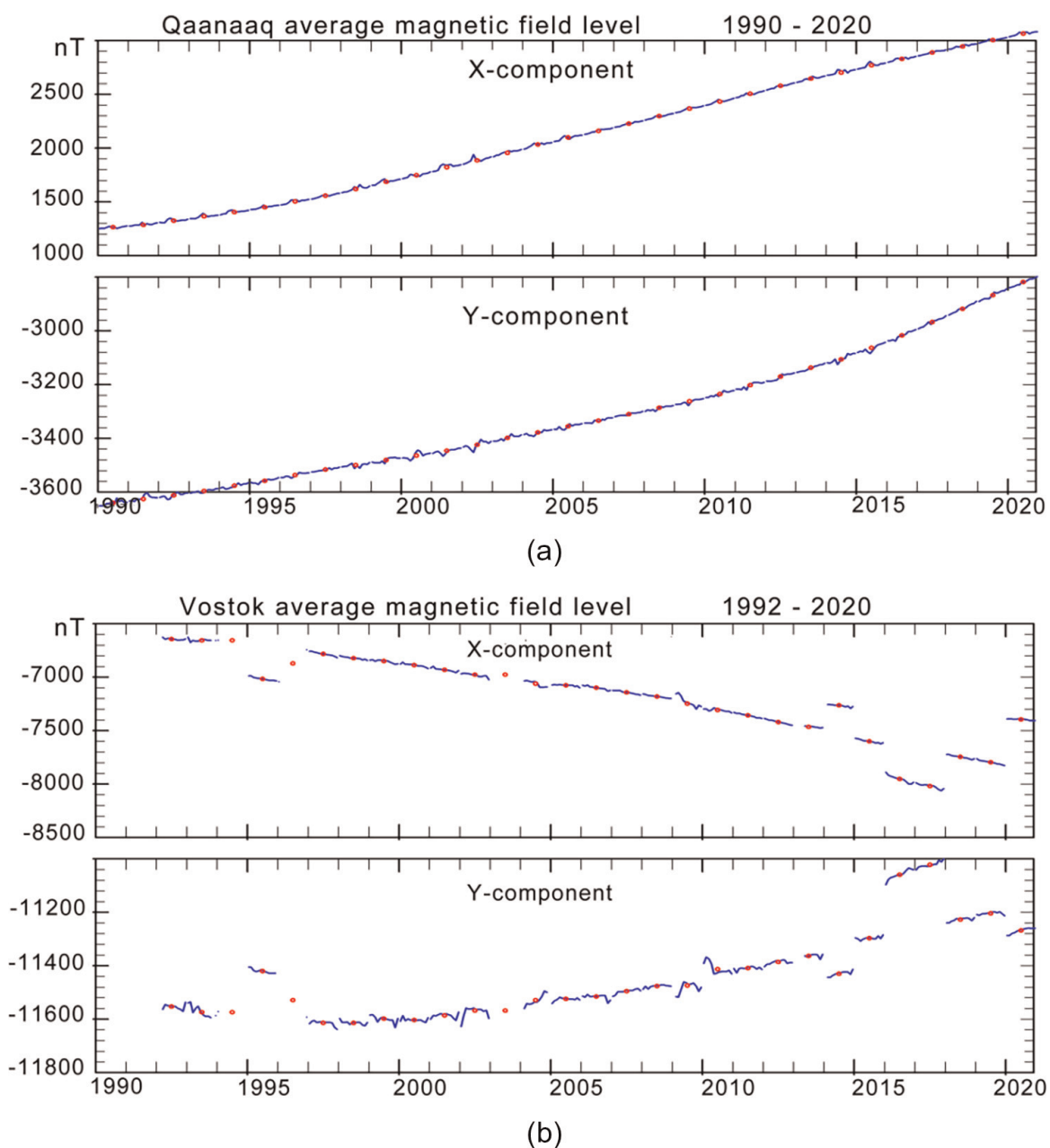
Figure 1.
*Monthly (blue line) and yearly (red dots) average X- and Y-component values compiled throughout all hours of
the 5 quietest days each month (http://isgi.unistra.fr). (a) Qaanaaq (THL) and (b) Vostok (VOS) (data from h
ttps://intermagnet.org and http://www.wdc.bgs.ac.uk).*

components. In the present work, the components are expressed in their (X,Y) representation, with X being the geographical northward component and Y the eastward component. Horizontal components in their geomagnetic representation or expressed by magnitude, *H*, and declination, *D*, could be used as well.

The definition of the level from which the magnetic variations should be measured is a controversial issue with different concept used by different PC index versions such as [12, 13, 41], or [42]. In the PC index version used, among others, in [17], the definition of the "solar rotation weighted" (SRW) reference-level construction published in [16] returns to the statements in [12, 13] with the vector formulation shown in Eq. (2) here and to the methods outlined in [43].

The essential point for the SRW method is deriving the reference level from quiet samples collected at conditions otherwise as close as possible to those prevailing at the day of interest. The factors of primary importance are:

i. Sample "quietness"

ii. Separation of the date of quiet samples from the QDC date

iii. Solar wind conditions (particularly IMF B_Y and V_{SW})

iv. Solar UV and X-ray illumination (based on solar radio flux F10.7 values)

For these factors, weight functions are defined to optimize the selection of samples for the QDC construction. For each hour of the day, observed hourly average values at corresponding hours within an extended interval (± 40 days) are multiplied by the relevant weights, added, and then divided by the sum of weights to provide the hourly QDC value. Subsequently, the hourly QDC values are smoothed to remove irregular fluctuations and interpolated to provide any more detailed resolution, such as 1-min values, as required.

The weight function (i) for sample quietness is determined from the variability of 1-min data samples within the hour much like the technique used in [12, 13] and detailed in [43]. Two parameters are calculated on a vector basis. One is the maximum time derivative used to indicate the smoothness within the sample hour. The other is the average variance to define the slope of data values. Both the parameters need to take small values for the hourly sample to be considered "quiet" (flat and featureless display).

For an estimate on a statistical basis of further weight functions (ii)–(iv) related to the solar rotation, the factors of importance were subjected to autocovariance analyses versus separation between the date of the QDC and the dates of the quiet samples to be included in the construction of the QDC values. The autocovariance values should take large values to meet the condition that the quiet samples used to build the QDCs must represent conditions as close as possible to those prevailing at the day of interest. Particular attention should be given to variations in the IMF B_Y component associated with the solar wind sector structure.

The details of the autocovariance analysis are provided in [16]. The main results were, as could be expected, high autocorrelation values at nearby dates and also high values at dates displaced one full solar rotation of 27.4 days from the day of interest. On these days, the solar illumination and the solar wind conditions, such as the solar wind speeds and the solar sector structure (at two-sector structures), were similar to the prevailing conditions on a statistical basis. In between, at half a solar rotation,

mixed IMF B_Y autocovariance results were found. In some cases, a local maximum was seen indicating the occurrences of four-sector solar wind structures. However, in most cases, the autocorrelation function had a deep minimum at half a solar rotation indicating two-sector structures. From these results, the above weight functions (iii) and (iv) were defined to take fixed values [16] making the QDC construction independent of parameters other than the measured polar magnetic variations.

Thus, at any time after initial 40 days of data collection, the relevant real-time QDC could be calculated, and after further 40 days of initial data collection, the final QDCs could be calculated for any day in the past. The hourly component averages and their quietness weight factors are fetched from their stored values, and their separation weight factors are found from the tabulated values. For each UT hour of the day, the hourly average component values within ±40 days are multiplied by the weight factors and summed up. The weight factors are summed up. The sum of weighted component hourly average values divided by the sums of weights defines for each hour the QDC value. The hourly sums of weights are quality factors for which alert limits could be set to caution against invalid values. The hourly QDC values are smoothed to remove fluctuations and then interpolated to provide the desired time resolution. The derived QDCs are routinely displayed in plots like those of **Figure 2a** and **b**.

In these diagrams for the X-components of the magnetic data from Qaanaaq (THL) and Vostok (VOS), there is a QDC curve for each day of the year. The daily QDC curves are drawn on top of each other in blue line for one month at a time. For day 1 (in black line), day 15 (yellow), and last day of the month (in red line), the QDCs are redrawn on top of the other QDCs. The additional curves provide an impression of the development of the QDCs throughout the month. The seasonal variations are very distinct in the developments of the monthly superposed QDCs with amplitude maxima at local summer. Most of the additional variability in the QDCs is caused by the IMF B_Y-related solar sector effects, which are then taken into account in the generation of appropriate daily QDCs. The displays of the Y-component QDCs are similar to the X-component displays.

The weighting over ±40 days makes the determination of the final QDC fairly insensitive to the intervals of missing data. Thus, the weighting technique allows the calculations of real-time QDCs with reduced accuracy from past data collected within −40 to 0 days (actual time) by simply ignoring the not yet available post-event samples without otherwise changing the ±40 days' calculation scheme. The QDCs could be improved gradually as new data arrive to be completed after passing +40 days with respect to the day of interest. Thus, with the predictable secular variations and the SRW-based QDC calculations defined here, there are seamless transitions between real-time and post-event QDC values.

5. PC index relations to the interplanetary merging electric field

With the methods for preparing the polar magnetic field variations defined in Section 4 and the formulas defined in Section 3, it is now possible to derive polar cap index values in post-event as well as in real-time versions. The PC indices are defined to match the merging electric field on the average throughout the reference epoch, which is 1997–2009 for Qaanaaq- and Vostok-based PCN and PCS values here. However, the question remains how well the PC indices match the merging electric field in specific cases and on different time scales.
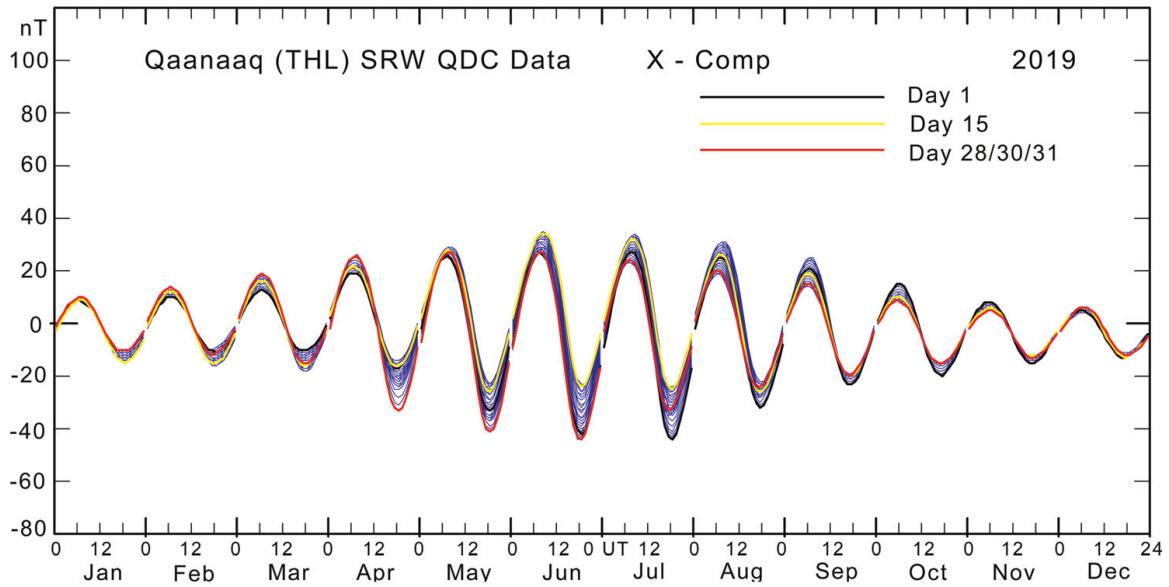
(a)
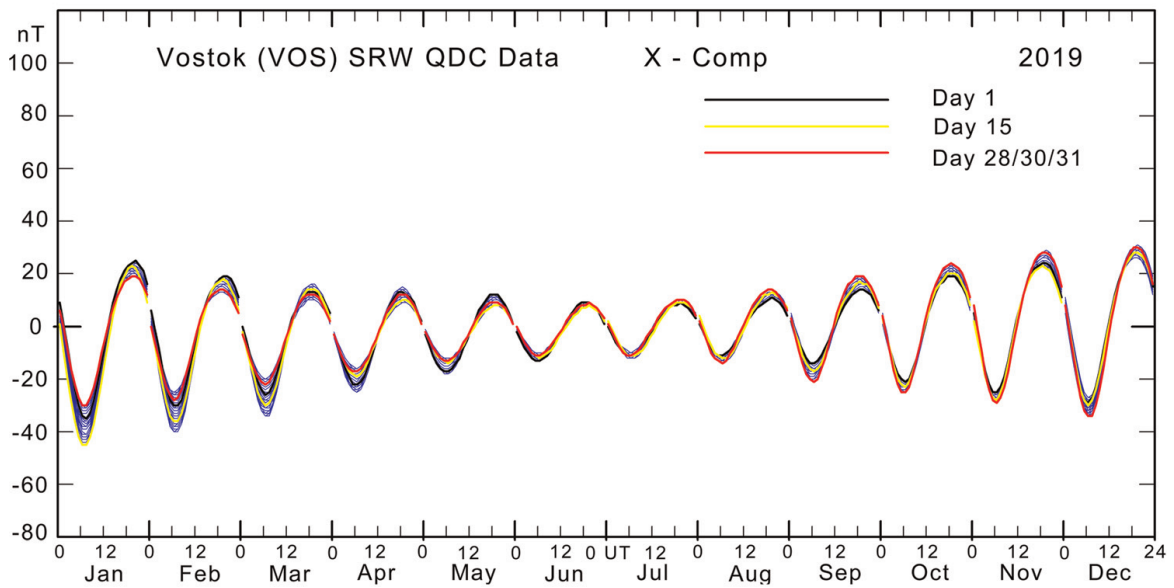
(b)

Figure 2.
QDC values for the X-components for Qaanaaq (THL) and Vostok (VOS) derived by SRW calculations. The monthly assemblies of QDCs are displayed in blue line. The variations on day 1, 15, and the last day of the month are superposed in black, yellow, and red lines, respectively.

In [29], the relations of the polar cap indices, PCN, PCS, and PCC, to the merging electric field, E_M [Eq. (3)], in the solar wind was investigated for the years from 1992 to 2018. The magnetic data supplied from INTERMAGNET (https://intermagnet.org) for Qaanaaq (THL) and Vostok were supplemented since 2009 by data from Dome-C observatory in Antarctica [39, 40]. The DMI2016 index calculation methods and coefficients [17] were used to derive index values.

Results from the correlations of PC index values in different versions with values of the merging electric field are displayed in **Figures 3** and **4**. The yearly average correlation coefficients are shown in **Figure 3**, where the coefficients for the correlation between PCN and E_M are displayed in blue line. The PCS-E_M correlation coefficients are depicted in red line, while the PCC-E_M correlation coefficients are shown by
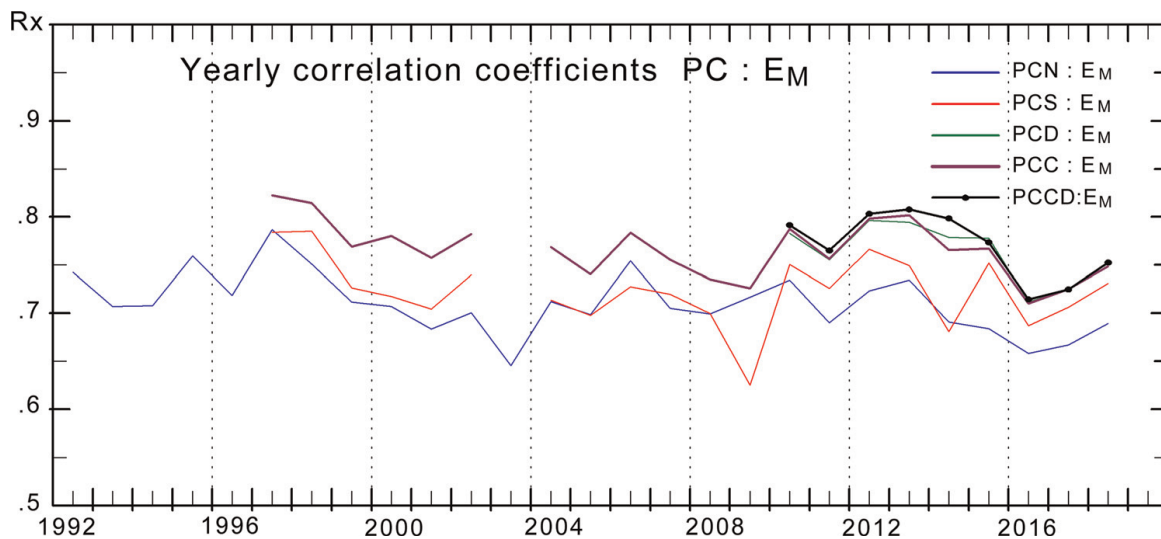
Figure 3.
Display of early averages of coefficients for the correlations between E_M and PCN (blue line), PCS-Vostok (red), PCS (PCD)-Dome-C (green), PCC-(Qaanaaq-Vostok) (heavy magenta), and PCCD-(Qaanaaq-Dome-C) in heavy black line (after [29]).
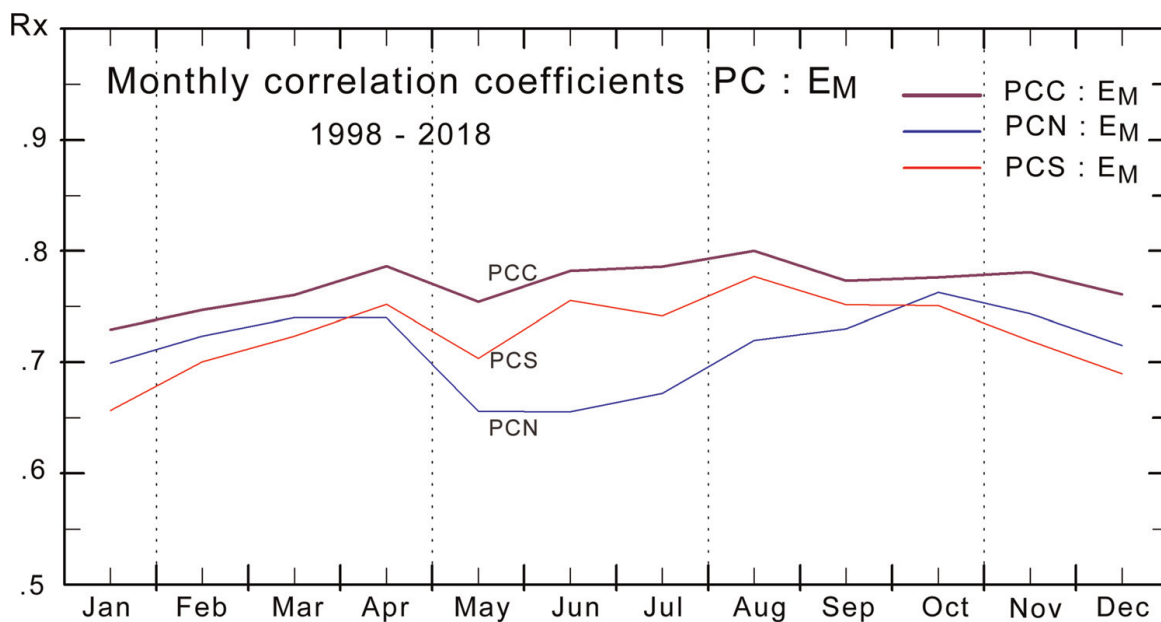
Figure 4.
Display of monthly average coefficients for the correlation between E_M and PCN (blue line), PCS (red), and PCC (magenta) (from [29]).

the heavy magenta line. In most cases, the PCC indices were derived from Qaanaaq-based PCN and Vostok-based PCS values. Data from Dome-C (DMC) observatory were used to derive an alternative PCS index, here denoted PCD, for the years 2012 and 2013, and further intervals where the Vostok data were incomplete. The correlation between E_M and PCD is displayed in green line, while the coefficients for correlation between E_M and PCC derived by using PCN and values of PCD substituted for PCS are displayed by the heavy black line named PCCD.

Figure 3 shows that the correlation between PCC and E_M is significantly higher than the correlation between E_M and either of PCN or PCS indices. It is also seen that the correlation between PCN and E_M is lower than the correlation between PCS and E_M with a few exceptions. It is seen from **Figure 3** that there is a tendency for

decreasing correlations between E_M and either of the PC indices with time over the recent years. An in-depth investigation of this issue is beyond the scope of the present work.

Figure 4 displays the average correlation coefficients for calendar months January-December based on values from the years 1998–2018 with exception of 2003 void of PCS data and 2013 with incomplete PCS data. Values for Dome-C available since mid-2009 only have not been included in the display in **Figure 4**.

The correlations between PCN and E_M shown in **Figure 4** are clearly lower in the northern summer months, May–August, than for the rest of the year. Similarly, the correlations between PCS and E_M are clearly lower in the southern summer months, November-January, for Vostok than for the other seasons. Selecting the local winter index, PCW, by jumping between the PCN and PCS traces at equinoxes, improves correlation values while selecting the local summer index (PCU) reduces correlations. The overall correlation between PCC and E_M is clearly higher throughout all years and all seasons than the correlations between E_M and either of PCN, PCS, PCA (average of PCN and PCS), PCW, and PCU index versions.

In summary, the PCC index is the preferred index version to use for solar wind magnetosphere interaction studies and for investigations of global magnetic disturbances such as auroral current systems and magnetospheric ring current relations.

6. Relations to auroral current systems

Part of the more steady ionospheric auroral current system is related to the magnetospheric plasma convection patterns and could be considered to flow as horizontal Hall currents in the transition region between the field-aligned currents from the magnetopause regions flowing downward at the dawn-side, upward at the dusk-side, and field-aligned currents flowing from the ionospheric regions to the ring current regime, upward at dawn, downward at dusk [44–47].

The steady auroral currents are at times strongly intensified by dynamic substorm-related horizontal currents flowing between sheets of field-aligned currents originating from instabilities in the magnetospheric tail current structure [48, 49].

The present work shall focus on the relations between polar cap indices and indices describing auroral current intensities such as the auroral electrojet indices AL (lower envelope of negative magnetic bays) and AU (upper envelope of positive bays, [50, 51]) and the corresponding SuperMag indices, SML and SMU, based on a wider selection of observatories [52]. These relations shall be looked at in terms of linear correlations and regression between series of index data and examination of conditions for the rapid enhancements of the auroral electrojet intensities associated with the onsets of substorm events.

The intensities of the (equivalent) horizontal ionospheric currents in the dawn sector are generally best described by the AL (or SML) indices, while the intensities of the horizontal ionospheric currents in the dusk sector are described by the AU (SMU) indices. The substorm-related currents in the midnight sector are best represented by enhancements in the AL (SML) indices.

The examples of such relations are displayed in **Figure 5a** and **b** for 5-min samples of AL and SML and PCN, PCS, and PCC indices throughout the 4-day interval from 16 to 19 March 2015. It is seen that there are close correspondence between the (negative) auroral indices in green line and the PCN indices in blue, the PCS indices in red, and, in particular, the PCC indices in magenta line.
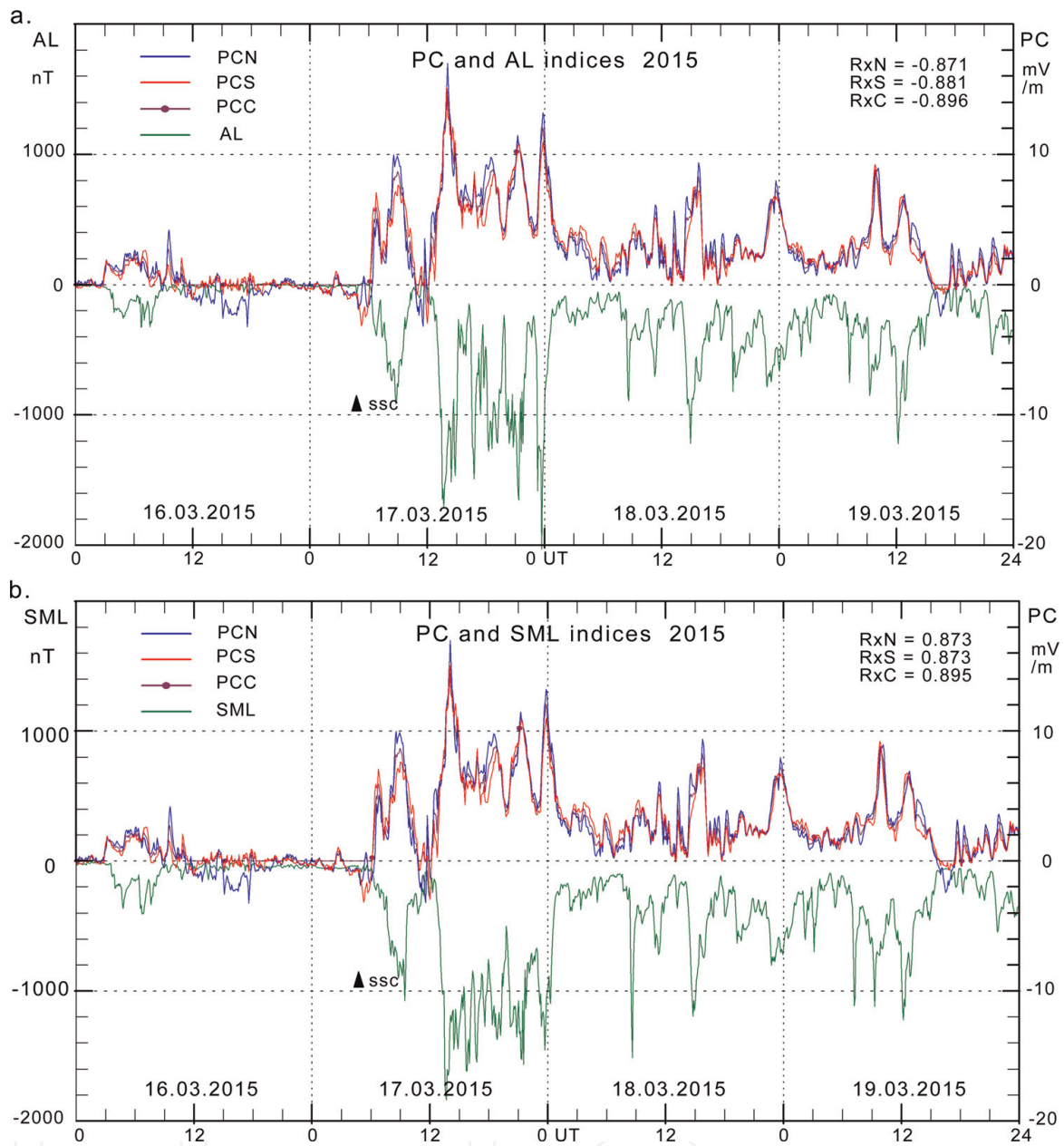
Figure 5.
(a) 5-min samples of PCN (blue), PCS (red), PCC (magenta), and AL (green) indices for 16–19 March 2015. Correlation coefficients are noted at the upper right section. (b) Corresponding display of PCN, PCS, PCC, and SML 5-min index samples for the same storm event.

There are several remarkable features in **Figure 5a** and **b**. The PCN, PCS, and PCC indices are almost identical except during the onset of the magnetic storm indicated by the sudden commencement on 17 March 2015 marked by the pointing (and size) of the black triangle marked SSC. The AL indices in **Figure 5a** are almost (negative) mirror images of the PCC values. The SML indices in **Figure 5b** indicate larger and sharper variations than the AL index values in **Figure 5a** probably due to the extended latitudinal coverage toward subauroral latitudes for the SML indices compared to observatory grid extent for the AL indices. The PCC-based correlation coefficients (RxC) noted in the upper right part of the figures are higher than the corresponding coefficients (RxN, RxS) for PCN or PCS, which speaks (again) for using the PCC over PCN or PCS indices in the examinations of large-scale geomagnetic disturbances.

The examples of statistical processing of a larger amount of auroral electrojet data shifted by 3 min versus corresponding PCC values are shown in **Figure 6a–d**. The correlation between the auroral and polar cap indices and parameters for the guiding regression lines are noted in the plots. The corresponding values based on further data sets are shown in **Figure 7**.

From **Figure 6a–d**, note the larger correlation coefficients for the SML and SMU versus PCC correlations than the corresponding correlations coefficients for the AL and in particular the AU indices versus PCC. The AU indices indicate stagnation for PCC indices beyond 5 mV/m probably because the range of observatories for the auroral electrojet (AE) indices misses the stronger AU-defining eastward electrojet events that move equatorward of the array of standard AE observatories.

Displays and calculations corresponding to **Figure 6** have been made for every year between 1997 and 2019 except 2003 where Vostok (or Dome-C) data were not available for PCS calculations. From these displays, the correlation coefficients and values of the slope and intercepts of the regression have been extracted in order to document their variations with time and solar cycle. The variations in correlation and slopes for SuperMag SML and SMU indices (equivalent of auroral indices, AL and AU) throughout 1997–2019 are displayed in **Figure 7**.

The ratio between amplitudes of 5-min AU, AL, and PCC indices similar to the ratio between SMU, SML, and PCC indices displayed in **Figure 7** have been used to
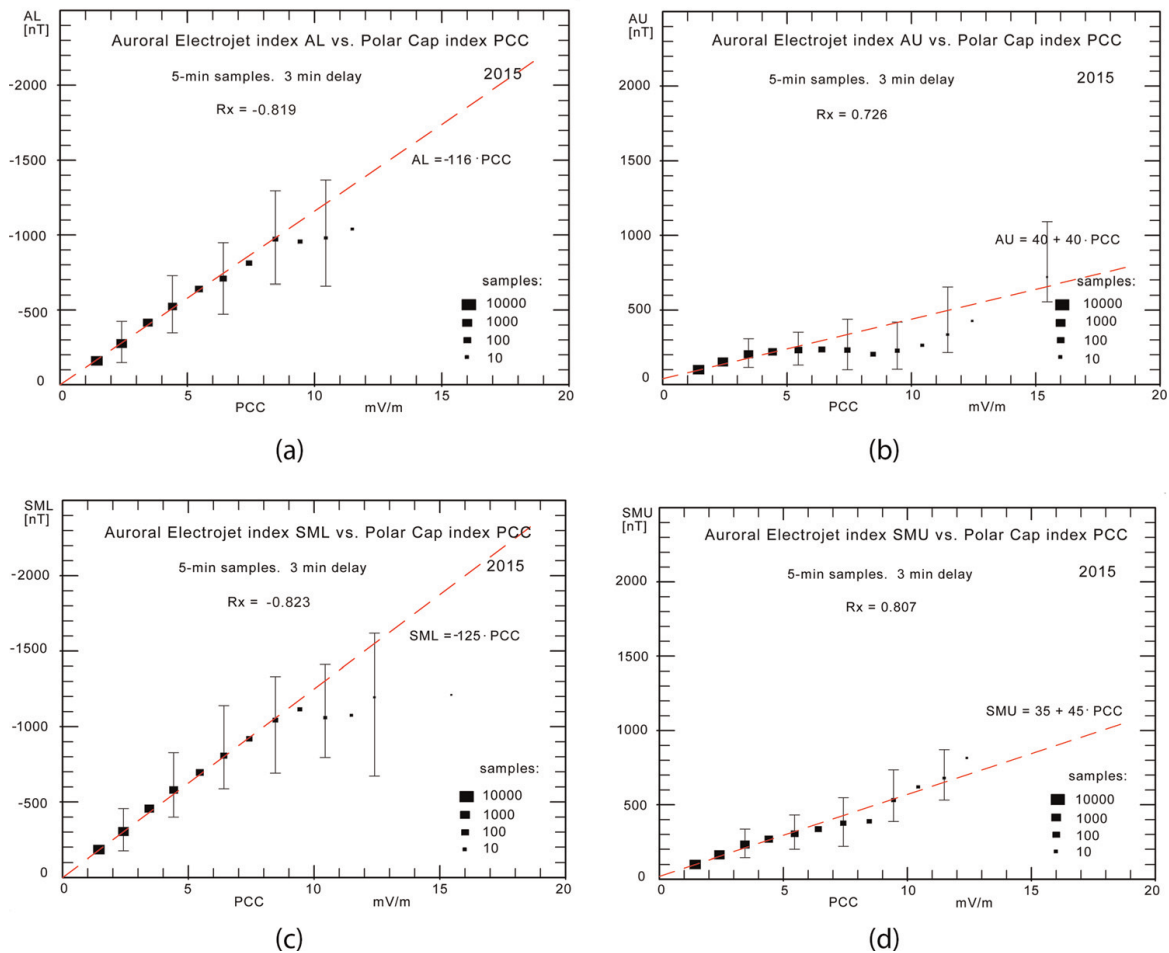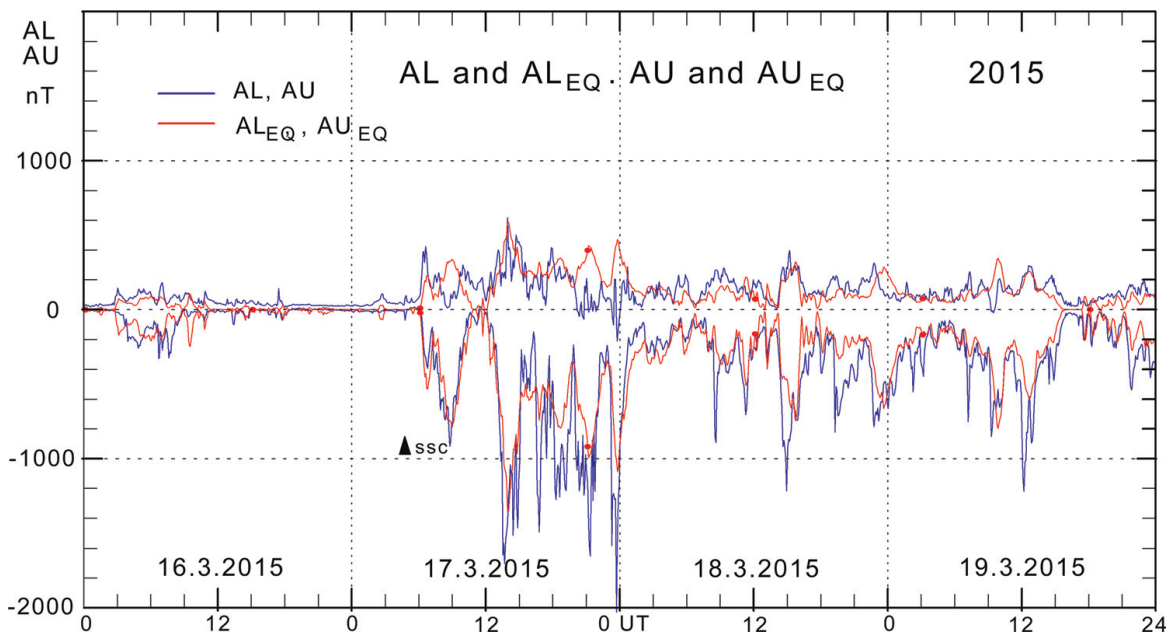

Figure 6.
(a) 5-min AL indices versus PCC. (b) 5-min AU indices versus PCC. (c) 5-min SML indices versus PCC. (d) 5-min SMU indices versus PCC. Correlation and regression results are noted in the diagrams.
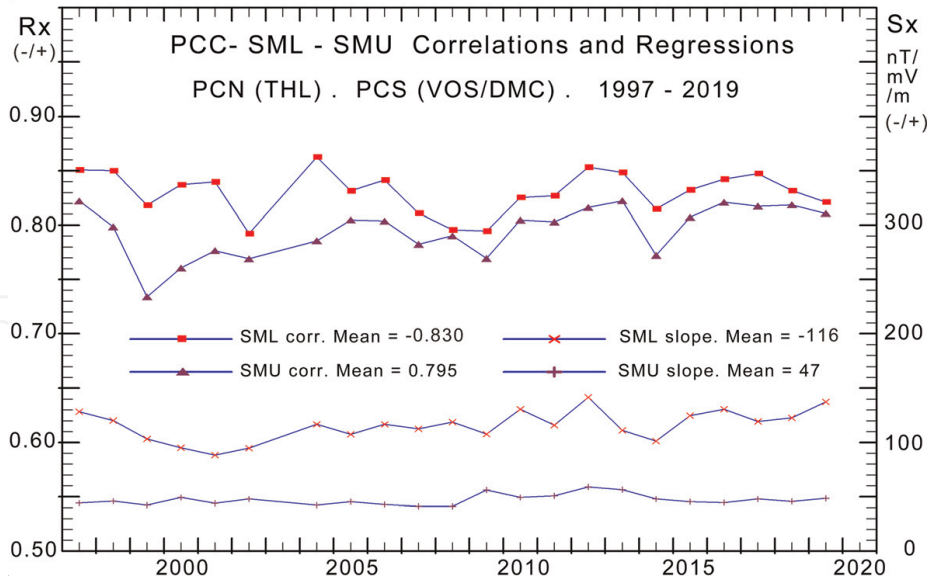
Figure 7.
From top: Yearly average correlations between 5-min PCC and SML (red squares connected by blue lines); yearly average correlations between PCC and SMU indices (magenta triangles); yearly average ratio between 5-min SML and PCC values (red crosses); and yearly average ratio between SMU and PCC indices (magenta crosses).

generate 5-min "equivalent auroral indices," AU_{EQ} and AL_{EQ}, from PCC indices. An example for March 2015 is shown in **Figure 8**.

Figure 8 displays a rather close agreement between the large-scale features of the electrojet, AL, indices and the PCC-based equivalent AL values, while the relations between the electrojet, AU, indices and the PCC-based AU_{EQ} values display less agreement. The use of equivalent auroral indices derived from values of the PCC indices may help to identify disturbances in recognizable appearances in real-time displays used at space weather monitoring. In addition, the conversion enables much closer examinations of the relations between series of the two different parameters, such as their average, absolute, and root-mean-square (RMS) differences, than

Figure 8.
Upper field: Display of 5-min AU index (blue line) and AU_{EQ} (red line) for 16–19 March 2015. Lower field: Display of AL (blue) and AL_{EQ} (red) indices.
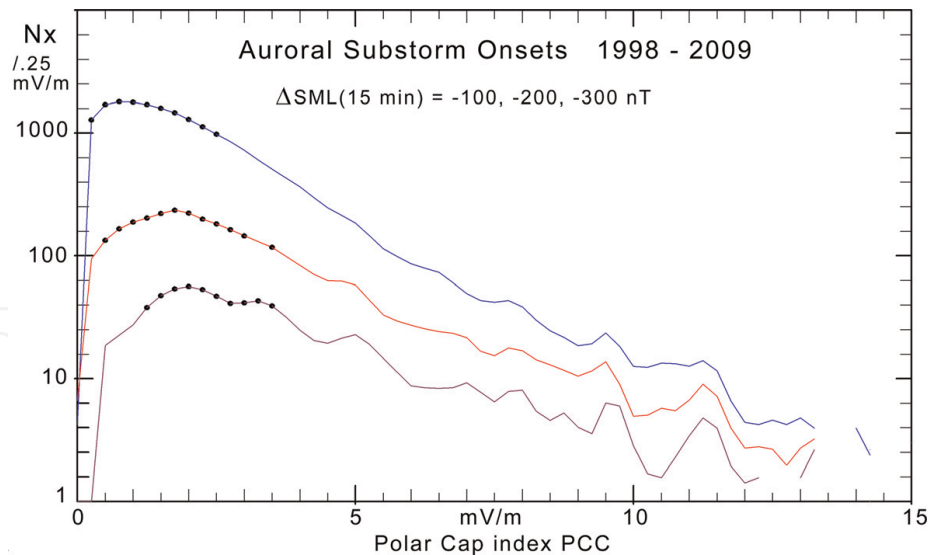
Figure 9.
Number of substorm cases within PCC bins of 0.25 mV/m with SML index changes by more than −100 nT/−200 nT/−300 nT in 15 min versus average PCC index values during the preceding 15 min.

available in just the correlation coefficients. These statistical results may help developing realistic physical models for the relations between solar wind parameters, transpolar plasma convection, and auroral current systems.

The prediction of substorm onset is a particularly intriguing issue. First, relevant substorm onset indications must be defined. There are widely different onset criteria depending on whether the developments in the mid-latitude positive bays [53] or the auroral negative bay [48] are used to identify substorm onsets. In the present work, a change in the 5-min auroral electrojet index, SML, by one of the amounts −100, −200, or −300 nT within 15 min are looked at. The average PCC index values within the preceding 15 min before the onset time are recorded. The number of counts within each bin of 0.25 mV/m in the PCC index is noted. The results from cases in 1998–2009 (ex. 2003) are displayed in **Figure 9**.

The dotted part of the −100 nT curve in **Figure 9** displays the amount of cases above half the top value (1871). This range corresponds to substorm pre-onset levels between PCC =0.25 and 2.25 mV/m. This range is broader particularly in the low-level limit than the range of 1.5 ± 0.5 mV/m suggested, among others, in [24] based on the same identification of substorm onset as the criteria used here. The dotted parts of the −200 nT and −300 nT curves indicate, correspondingly, the amount of cases above half the top values of their occurrence patterns.

7. Relations between PC indices and the partial ring current system

The partial (asymmetric) ring current indices, ASY-H and ASY-D, are provided by Kyoto WDC-C2 [51] as 1-min values. Here, the study shall focus on the relations between ASY-H indices and the polar cap indices, PCC. The 1-min samples of both series have been averaged to form 15-min samples. Using a stepwise variable delay between samples of the respective time series, the 15-min index data sets have been subjected to linear correlation analyses assuming that the maximum value of the correlation coefficient provides the most appropriate delay. With this delay imposed on all the pairs of samples of the time series, linear relations between the two

parameter sets were found by least squares regression. The average deviation, the average numerical (absolute) deviation, and the RMS standard deviation were calculated from the assumed linear relations.

The reported investigations have considered 4-day intervals of all the major geomagnetic storms with Dst(peak) < –100 nT with onsets from quiet conditions on the first day and occurring during the interval from 1992 to 2018. **Figure 10** displays a scatter plot of 15-min ASY-H index values against PCC values. The number of individual samples for each unit interval in PCC is illustrated by the size of the black squares on the (logarithmic) scale shown in the lower right section of the display. In order to avoid cluttering the display, standard deviation values are shown by the error bars plotted in every other interval only. The 8-min delay noted in **Figure 10** was found to provide least RMS deviation and optimum correlation (Rx = 0.743) for the regression between 15-min samples of the two index series.

A noteworthy feature in the display is the persistent closely linear relation between the average ASY-H and PCC index values up to high disturbance levels. The relation is expressed as

$$ASY-H = 10.9 \cdot PCC + 16 \text{ [nT]}. \tag{9}$$

The number of 15-min samples, correlation coefficients, and results from the linear regression analyses for various PC index versions are summarized in **Table 2** [from [29]]. In addition to presenting PCN, PCS, and the combination PCC [cf. Eq. (8)], the table comprises PCA, which is the plain average of PCN and PCS, and the seasonal selections PSW (local winter) and PCU (summer).

It should be noted that data for the various versions have been selected from the epoch 1992–2018 on the basis of the magnetic storm intervals. Hence, no effort was made to avoid intervals where data for one or the other index version were missing. Note, in particular, the reduced number of PCS samples due to intervals of missing or invalid Vostok data (cf. **Figure 1b**).
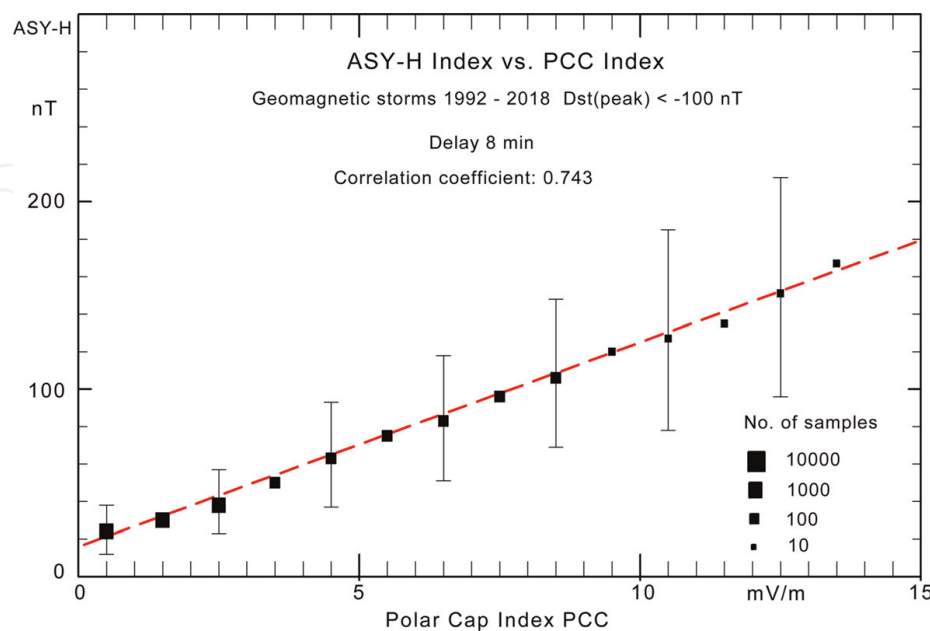
Figure 10.
Scatter plot of ASY-H against PCC index values. The black squares indicate average values and the number of 15-min samples within each unit interval in PCC, while the error bars at every other unit interval indicate standard deviation. The red-dashed line indicates least squares regression slope and offset values for the 15-min data samples [Eq. (9)]. [from [29]].

Version	PCC	PCN	PCS	PCA	PCW	PCU	Unit
Samples	28,803	34,839	28,802	28,880	33,728	29,913	
Correlation	0.743	0.702	0.679	0.716	0.700	0.683	
Mean dev.	–1.7	–0.3	–0.8	–0.5	0.1	–0.6	nT
RMS dev.	23.6	24.5	25.6	24.0	24.0	25.5	nT

Table 2.
Number of samples, correlation coefficients, and regression results for ASY-H/PC relations [from [29]].

While the correlation coefficient for 15-min samples of the PCC-ASY-H relation in **Figure 10** is Rx = 0.743, then the correlation between the ASY-H and further PC index versions is all close to correlation coefficient values of only around Rx = 0.70. The problem resides, in particular, with the negative PC index values since the ASY-H values are dominated by positive index values.

The linear relation between ASY-H and PCC could be used to generate an "equivalent ASY-H index," ASY-H_{EQ}, based on rescaling the PCC indices according to Eq. (9). This would provide basis for close comparisons of the two index series by enabling the calculations of parameters such as mean, absolute, and RMS deviations at various conditions. The calculation of equivalent values might, furthermore, generate a display of ASY-H_{EQ} looking much like displays of the real ASY-H indices, which could be useful for monitoring the asymmetric ring current developments in real-time applications where the PC indices are available online in their real-time version. The examples of real (published) ASY-H indices and PCC-based ASY-H_{EQ} indices are displayed in **Figure 11a** and **b** for the magnetic storm events of 16–19 March 2015 and 22–25 June 2015, respectively.

Comparing ASY-H (magenta line with dots) with ASY-H_{EQ} (red line) in the upper fields of **Figure 11a** and **b** indicates a moderate degree of agreement, which is best at the onset phase of the displayed magnetic storms starting on 17 March 2015 and 22 June 2015, respectively. The direct conversion of PCC indices to equivalent SYM-H values shown in the lower fields is not working well (see Section 8).

8. Relations between PC indices and the symmetrical ring currents

The intensity of symmetrical ring currents can be monitored by the hourly ring current index, Dst, and more detailed by the 1-min SYM-H indices provided by Kyoto WDC-C2 [51, 54]. The relations between series of polar cap indices and SYM-H (or Dst) indices using a variable delay (PC indices leading) have failed to generate maximum correlation at time shifts by up to 4 h [29]. Instead, the approach suggested in [27, 28] is applied here. Thus, the PCC index is used in a source function for the gradient in the Dst index rather than in correlations with its actual values.

The Dst index [55] is considered to represent the amount of energy stored in the ring current by the Dessler–Parker–Sckopke relation [56, 57]. Following Burton et al. [58], the rate of change in the Dst* index with time could be written as

$$dDst^*/dt\ [nT/h] = Q[nT/h] - Dst^*[nT]/\tau\ [h]. \qquad (10)$$

Here, Dst* is the Dst index corrected for contributions from magnetopause currents (MPC). The quantity Q (in nT/h) is the source term, while the last term in
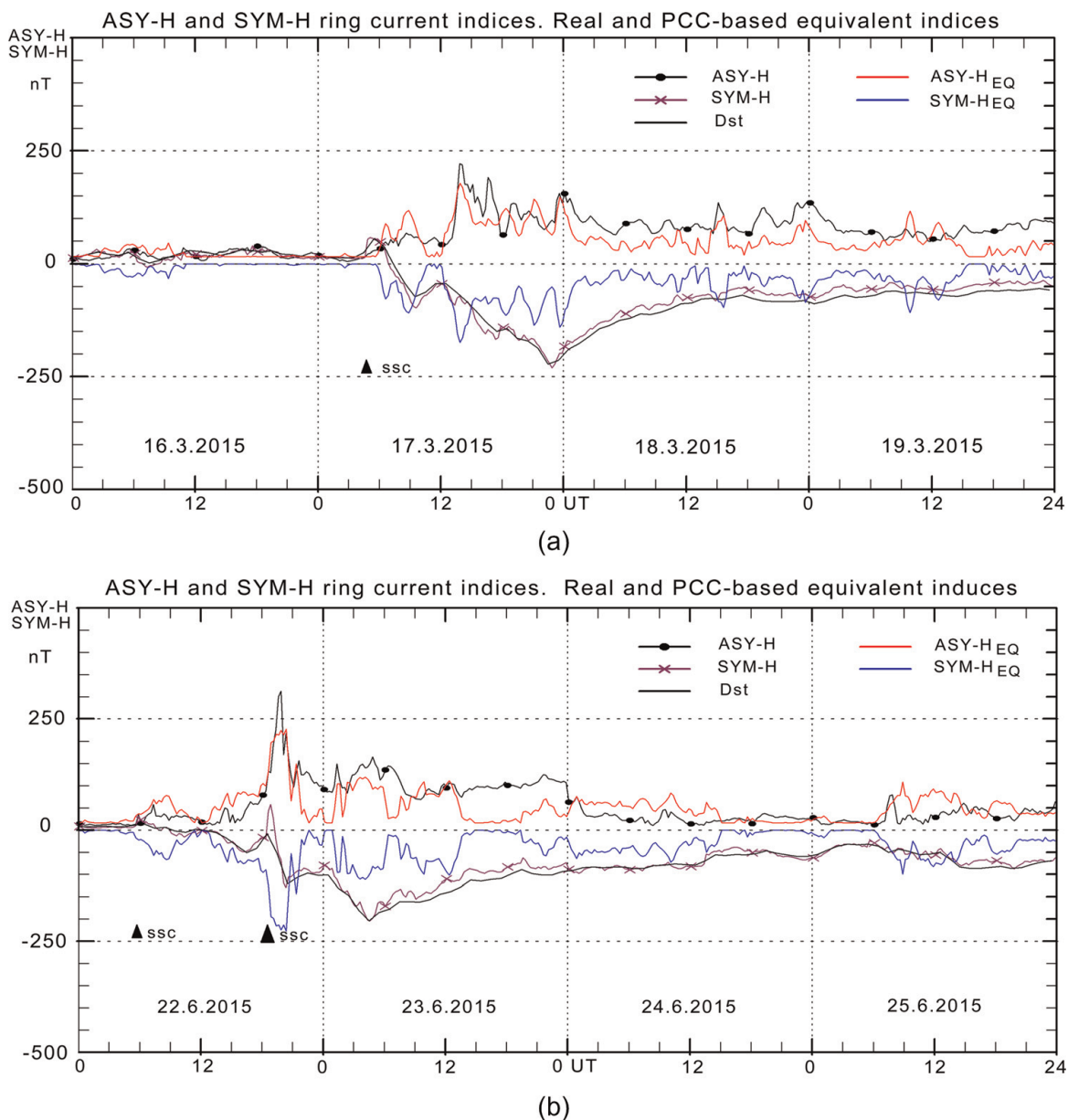
Figure 11.
Magnetic storms (a) 16–19 March 2015 and (b) 22–25 June 2015. The upper part of the fields display real (published) ASY-H indices (black line with dots) and equivalent ASY-H_{EQ} values (red) converted from PCC index values by scaling [Eq. (9)]. The lower parts display real (published) SYM-H (magenta line with crosses) and Dst indices (black line), and equivalent SYM-H_{EQ} index values (blue) converted from PCC indices by scaling. The triangular symbols mark events of storm sudden commencements (SSC).

Eq. (10) is the ring current loss function controlled by the decay time constant, τ, [59]. For the small actual MPC corrections, the Dst-dependent statistical values provided in [60] are used here. For further details, see [29]. Now, the relation in Eq. (10) has only terms relating to the source function Q and may provide equivalent Dst index values by integration from a known state, once the source term is defined.

In [58], the source term Q was related to the Y_{GSM} component of the solar wind electric field. In the analyses by Stauning et al. [27] and Stauning [28], the relations of Q to the polar cap indices were examined for a number of storm event cases during the intervals 1995–2002 and 1995–2005, respectively. These analyses were extended in [29] to comprise selected large storm events with Dst(peak) < –100 nT and storm onset on the first day throughout 1992–2018 in order to improve the statistical basis. The temporal change at time t = T in the hourly Dst* index were

derived from the hourly values at t = T – 1 and t = T + 1 [h] by the simple differential term:

$$dDst^*/dt(T\,h) = (Dst*(T+1\,h) - Dst^*(T-1\,h))/2. \tag{11}$$

In **Figure 12**, hourly values of dDst*/dt derived from archived data using Eq. (11) and corrected for decay (Eq. (10); [59]) have been plotted against the related PCC index values. Average values within each unit of PCC are displayed by the black squares with sizes corresponding to the number of hourly samples according to the lower right scale, while standard deviation is marked by error bars (in every other bin).

The scatter plot in **Figure 12** presents variations in the Dst* source function, Q_{OBS}, with PCC using a variable time shift to obtain the best correlation. The relation between the best fit source function, Q_{OBS}, and the source parameter values, PCC, is then expressed in a linear function. From the selected data set (98 storm periods within the interval from 1992 to 2018), the regression on the total amount of hourly samples provides the slope and offset values indicated by the red-dashed line in **Figure 12** and reported as follows:

$$Q_{OBS}\,[nT/h] = -4.1\,[(nT/h)/(mV/m)] \cdot PCC\,[mV/m] - 2.2\,[nT/h]. \tag{12}$$

This result is close to the corresponding source function (Q = –4.6·PCC – 1.2) defined in Stauning [28] from a smaller amount of data (storm events 1995–2005).

With continuous time series of the PCC-based source values, and specifications of the relational constants and initial Dst values, it is now possible, at least in principle, to integrate Eq. (10) to derive the values of an "equivalent Dst index", Dst_{EQ}, throughout any interval of time. The reported work [29] has brought the analysis of the relations between Dst and the polar cap index, PCC, important steps forward compared to [28] by including a close examination of the decay time constants (τ = 5.8 h and τ = 8.2 h) in [59] and their turning level (DstXlevel = –55 nT), and other
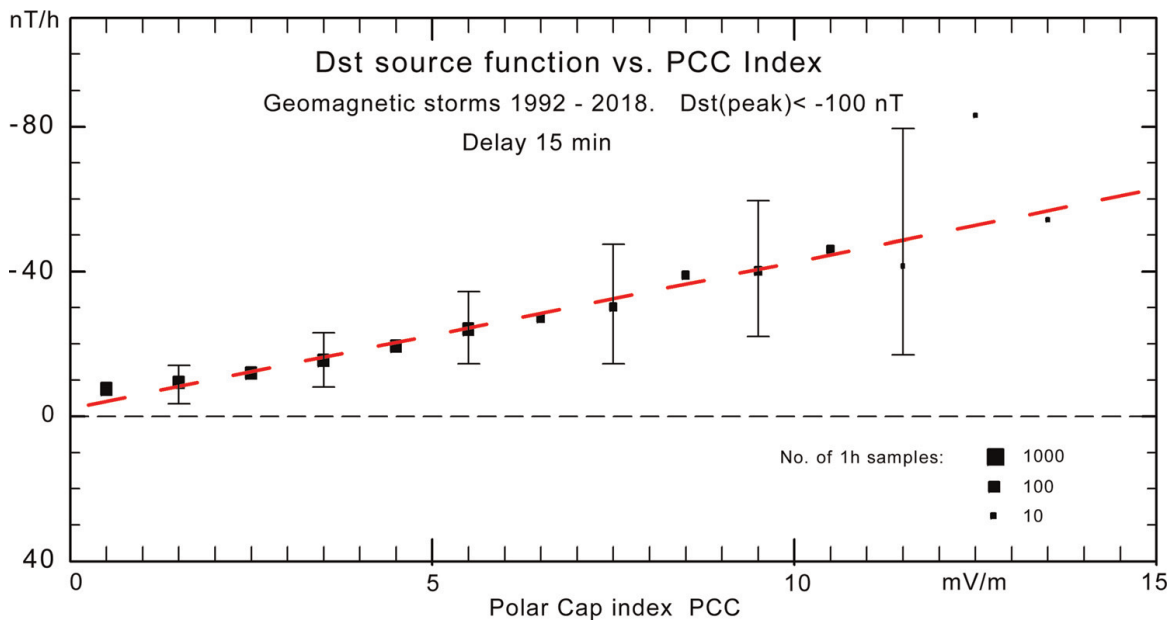
Figure 12.
Scatter plot of d(Dst*)/dt corrected for decay versus polar cap PCC index. The black squares represent bin-average values and no of hourly samples, while the error bars in every other bin represent standard deviations (from [29]].

parameters of importance for the relations between Dst and its possible source functions, primarily the PCC index. A further parameter introduced here is the optimum delay between samples of the PCC time series and the Dst values. For these cases, the PCC-based index values lead by a few ($\approx$45) min.

In addition to the decay time constants [59], the examination included the impact from the saturation [61] of the PC indices at high levels of the merging electric field, E_M, as seen in all PC index series [18].

In a crude approximation for the parameter iteration process, an "effective PCC index" (PCCeff) were set equal to the E_M values up to a turning level (PCClim) at around 5 mV/m and then forced to deviate by adding a linearly varying term with slope (S) less than unity. The approximation is defined by the two-step linear relation as follows:

$$\text{PCCeff} = \text{PCC for PCC} < \text{PCClim} \tag{13}$$

and

$$\text{PCCeff} = \text{PCC} + \text{Seff} \cdot (\text{PCC–PCClim}) \text{ for PCC} > \text{PCClim} \tag{14}$$

where Seff = $(1/S – 1)$ is less than unity.

The above-mentioned set of 98 magnetic storms with peak Dst below –100 nT occurring throughout the epoch from 1992 to 2018 where PCS indices are available (with some gaps) was used as a testbed to explore the effects of parameter adjustments. For the calculation of PCN indices, Qaanaaq (THL) data have been almost continuously available since 1975. Dome-C magnetic data have been substituted for missing or unreliable Vostok data (cf. **Figure 1b**) for PCS calculations, among others, throughout 2012 and 2013. For each storm event, a sequence of 4 days is considered at a time with the storm beginning from quiet conditions on the first day. Starting from the initial decay time values defined in [59], the source values defined in Eq. (12), and the PCC values modified according Eqs. (13) and (14), the parameters were changed in small successive step searching for maximum correlation and minimum deviations between real and equivalent Dst values.

The examples of observation-based and equivalent Dst values are displayed in **Figure 13a** and **b**. For these cases, the integration of the source term has been started at the real Dst value and then allowed to proceed independently throughout the 4 days in each set.

The examples in **Figure 13a** and **b** were based on using PCC indices in the source function for possible applications of the technique at space weather monitoring. They represent cases (a) of high correlation (Rx = 0.957) and (b) moderate correlation (Rx = 0.762) compared to the average correlation level (Rx = 0.810) for the selection of storm events. A specific feature of **Figure 13b** is the effects of the strong storm sudden commencement (SSC) at 15 UT on 22 June 2015. The occurrences of SSC events counteract the ring current effects on low-latitude magnetic observations, thereby preventing the reported Dst index values from reaching the full (negative) peak values corresponding to the actual ring current intensities displayed by the PCC-based Dst_{EQ} index series, which is less sensitive to SSC effects.

Figure 13a and **b** indicate very good and fair agreement, respectively, between the real and the equivalent Dst values. Generally, the agreement is best for moderate storms. Going from the moderate to the strong storm cases gives sometimes less agreement between real Dst values and equivalent PCC-based Dst_{EQ} values, possibly related to saturation effects not compensated for by the PCC modifications defined in
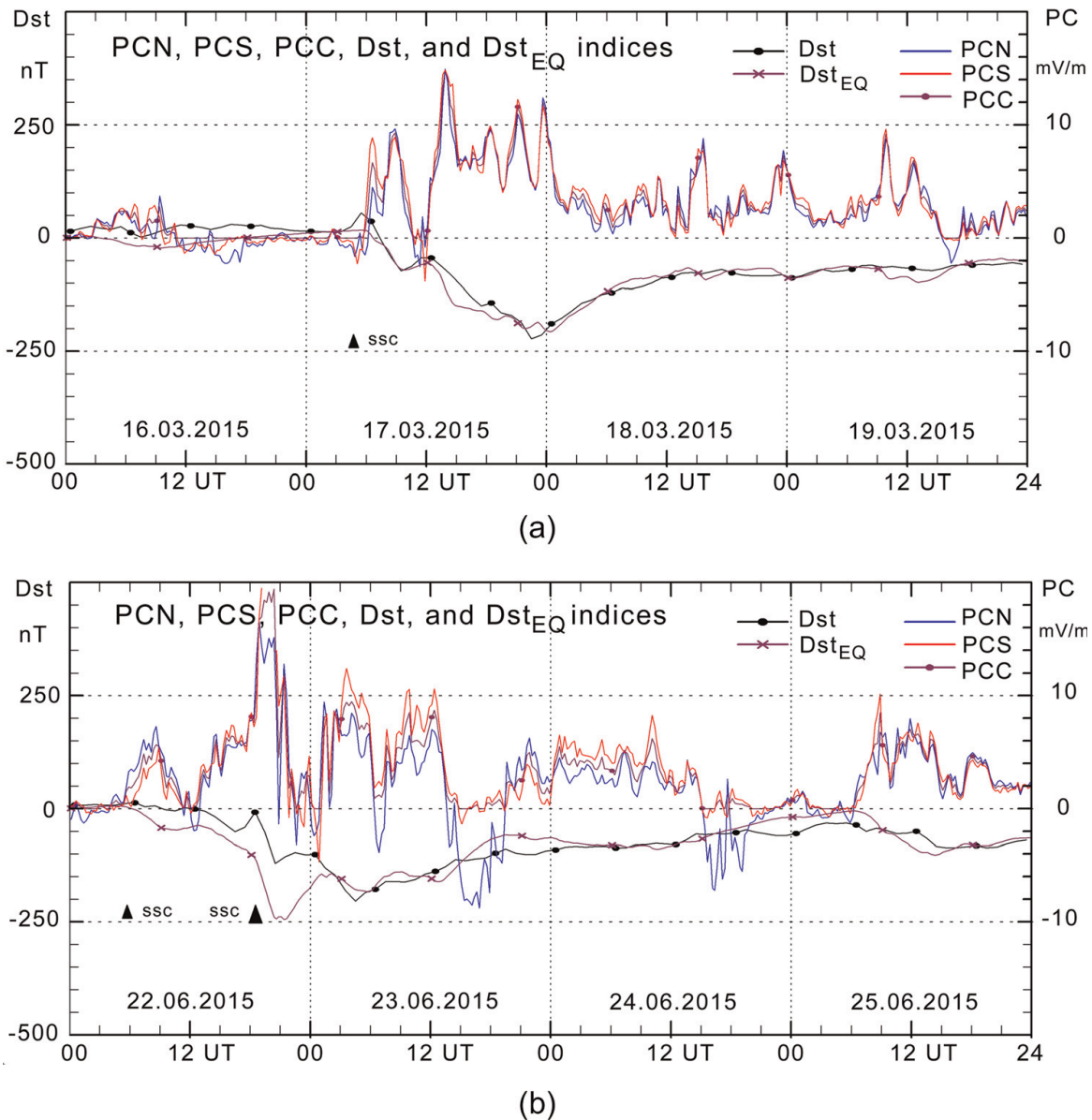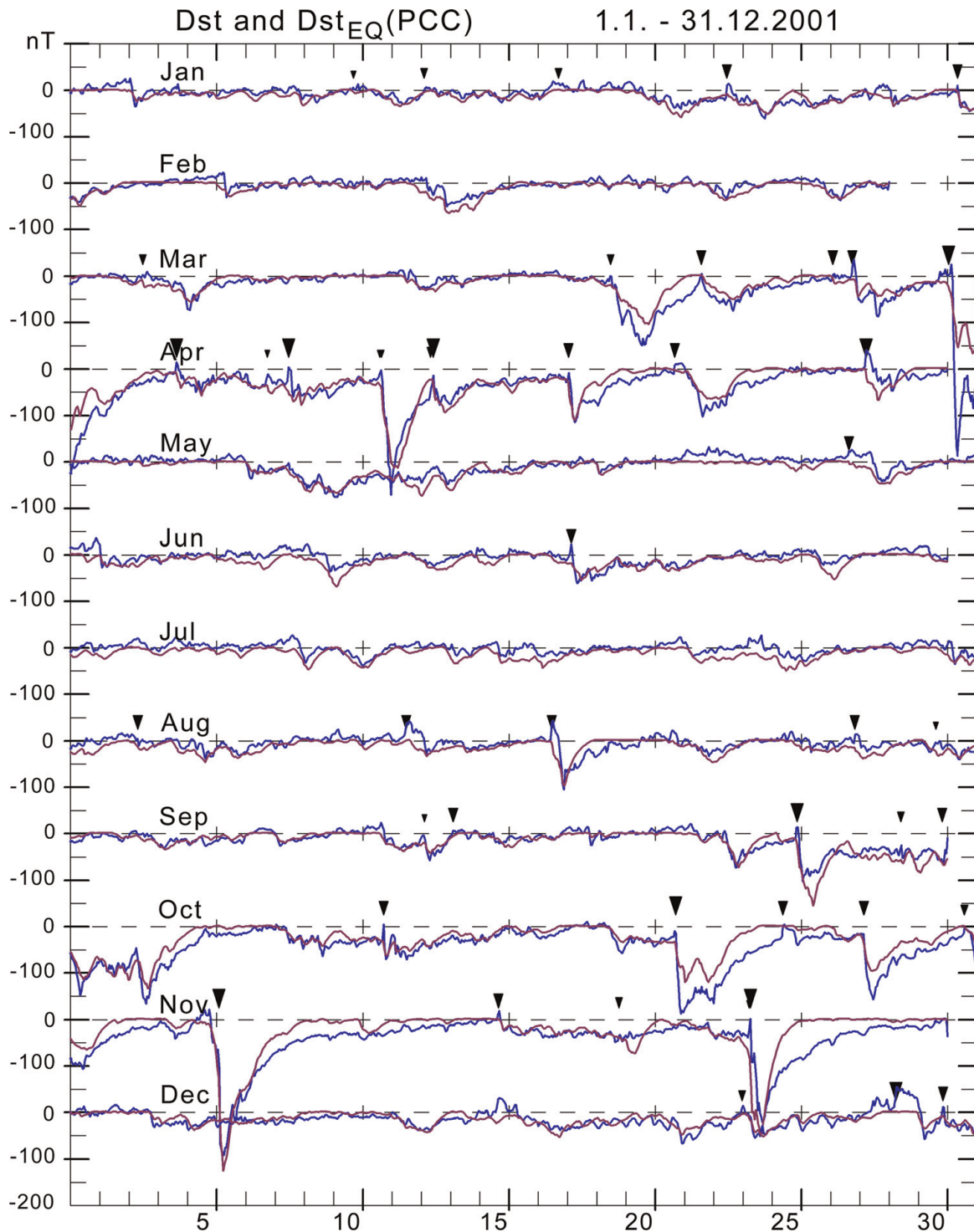
Figure 13.
(a, b) Examples of published (real) Dst (black line, dots) and equivalent Dst (magenta) values calculated from the PCC-based source function. Values of PCC (magenta), PCN (blue), and PCS (red) are displayed in the upper fields on the right scale [from [29]].

Eqs. (13) and (14). For the very weak cases, the uncertain influence from magneto-pause currents (MPC), although small, may have relatively large effects, which reduce the agreement between the real and the equivalent Dst indices.

With the understanding of the effects of adjustments of the various parameters gained from the test bed exercises, the full range of available data has been used to integrate the PCC-based source function throughout the epoch from 1992 to 2018 to derive equivalent Dst_{EQ} values without attachment at all to the published (real) Dst values. In cases where either PCN or (Vostok or Dome-C-based) PCS values were unavailable, the available hemispherical PC indices were used for PCC index calculations with degraded accuracy.

In the first step, the timing parameters were adjusted to provide the overall best correlation and least deviations related to values of decay time constants for the "fast" decay at high disturbance levels and "slow" decay at low disturbance levels as well as

Figure 14.
Observed Dst values (blue line) and calculated Dst$_{EQ}$ values (magenta) for 2001. Storm sudden commencement (SSC) events are displayed by the downward pointing black triangles to indicate onset times and sized to indicate their amplitudes [from [29]].

Dst values at the cross-over (DstXlevel). In a second step, the PCC high-level modifications suggested by Eqs. (13) and (14) were used to provide the best possible agreement between peak values of Dst$_{EQ}$ and Dst keeping the other parameters near their initial values. The iterations gave slightly different parameter values depending on the choice of quality parameters considered in the process. Thus, the final parameter values are not unique but represent compromises. For the control of the methods and calculations, the derived Dst$_{EQ}$ values have been displayed in plots along with the real

Symbol	Optimal	Unit
Fast decay, τ_1	5.5	h
Slow decay, τ_2	7.0	h
DstX level	−52	nT
Dst gradient	−4.5	(nT/h)/(mV/m)
PCClim	5.0	mV/m
PCCslope, S_{eff}	0.60	–
Delay $Dst_{EQ} - Dst$	45	min

Table 3.
Parameters for Dst_{EQ} calculations.

Result term	Optimal	Unit
Mean Dst	−13.08	nT
Mean Dst_{EQ}	−13.09	nT
Mean diff.	−0.01	nT
Abs. diff.	8.88	nT
RMS diff.	12.30	nT
Correlation	0.856	–

Table 4.
Results from Dst_{EQ} calculations.

Dst values throughout the entire epoch. Interim examples for the stormy year 2001 are displayed in **Figure 14**.

Figure 14 displays close, although not perfect, match between the real Dst values (blue line) based on observed near-equatorial magnetic variations and the equivalent Dst_{EQ} values (magenta line) calculated by the integration of the PCC-based source function [Eq. (10)] using the parameters estimated from the lengthy correlations throughout 1992–2018 including high-level modifications of the PCC indices. The integration was performed in steps of 5 min starting from $Dst_{EQ} = 0$ on 1 January 1992 using parameters listed in **Table 3**. A summary of results is listed in **Table 4**.

In **Tables 3** and **4**, the "Optimal" columns refer to parameters and results derived from the total 1992–2018 integration sequence [from [29]].

9. Real-time applications

When the relations discussed in the preceding sections are used in real-time applications, such as the monitoring and forecasts of space weather conditions, then it is necessary to derive the PC index parameters in real-time versions based on polar magnetic data assumed available in real time either directly from an observatory or from Internet links.

The scaling parameters are the same being independent on whether used for post-event or real-time calculation of PC indices. The secularly varying baseline values are

predictable to a high degree of accuracy. Thus, the problem resides with the QDC-level calculations.

As mentioned in Section 4, the solar rotation weighted (SRW) QDC method is very well suited for real-time applications. While maintaining the weight factor definitions, the calculation scheme is not changed by the transition from using quiet samples from the past 40 days up to the present hour neglecting post-event samples in real-time PC index calculations to using the full range of data from ±40 days for post-event index calculations.

The differences between the post-event and real-time PC indices were examined in [62]. **Figure 15a** displays in the upper two panels an example for 2015 of hourly PCS index values derived by using post-event (PE) and (simulated) real-time (SRT) methods, respectively. The bottom panel displays the differences. These differences are largest in the local summer months.

(a)

(b)
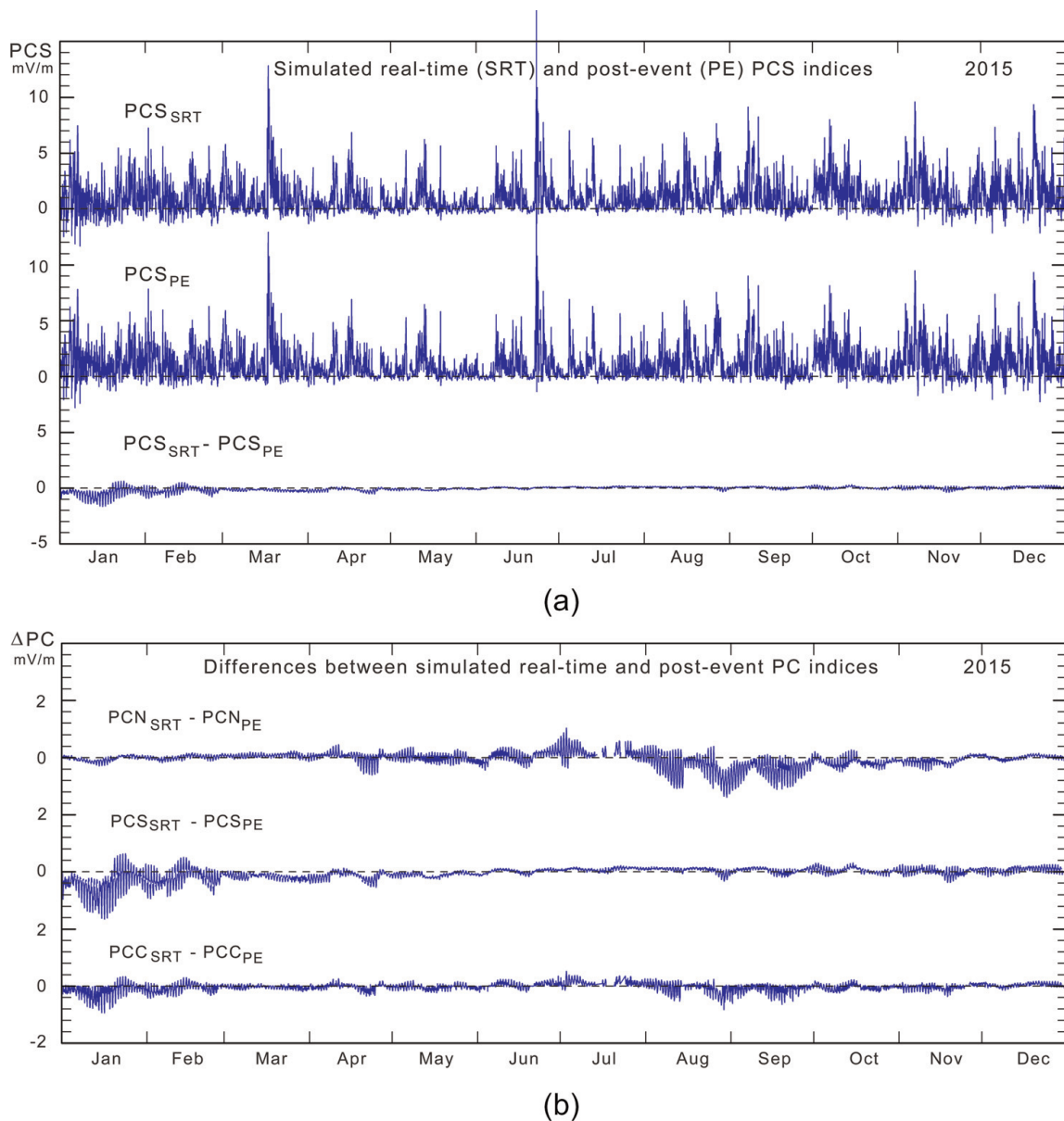
Figure 15.
(a) Simulated real-time (SRT) (upper part) and post event (PE) PCS (middle part) index values based on Vostok magnetic data using common calibration parameters and SRT or PE versions of QDC values, respectively. The lower part of the field displays their differences. (b) Differences between SRT-based QDCs and PE-based QDCs for PCN, PCS, and PCC indices [from [62]].

The differences for PCS have been transferred to the middle field of **Figure 15b** on a more sensitive scale. The corresponding calculations of differences were made for the PCN indices presented in the upper field of **Figure 15b** and for the PCC indices presented in the bottom field of **Figure 15b**. It is seen that the relatively small and seasonally dependent differences between the post-event and the real-time PCN and PCS versions are further mitigated when derived for the combined PCC index.
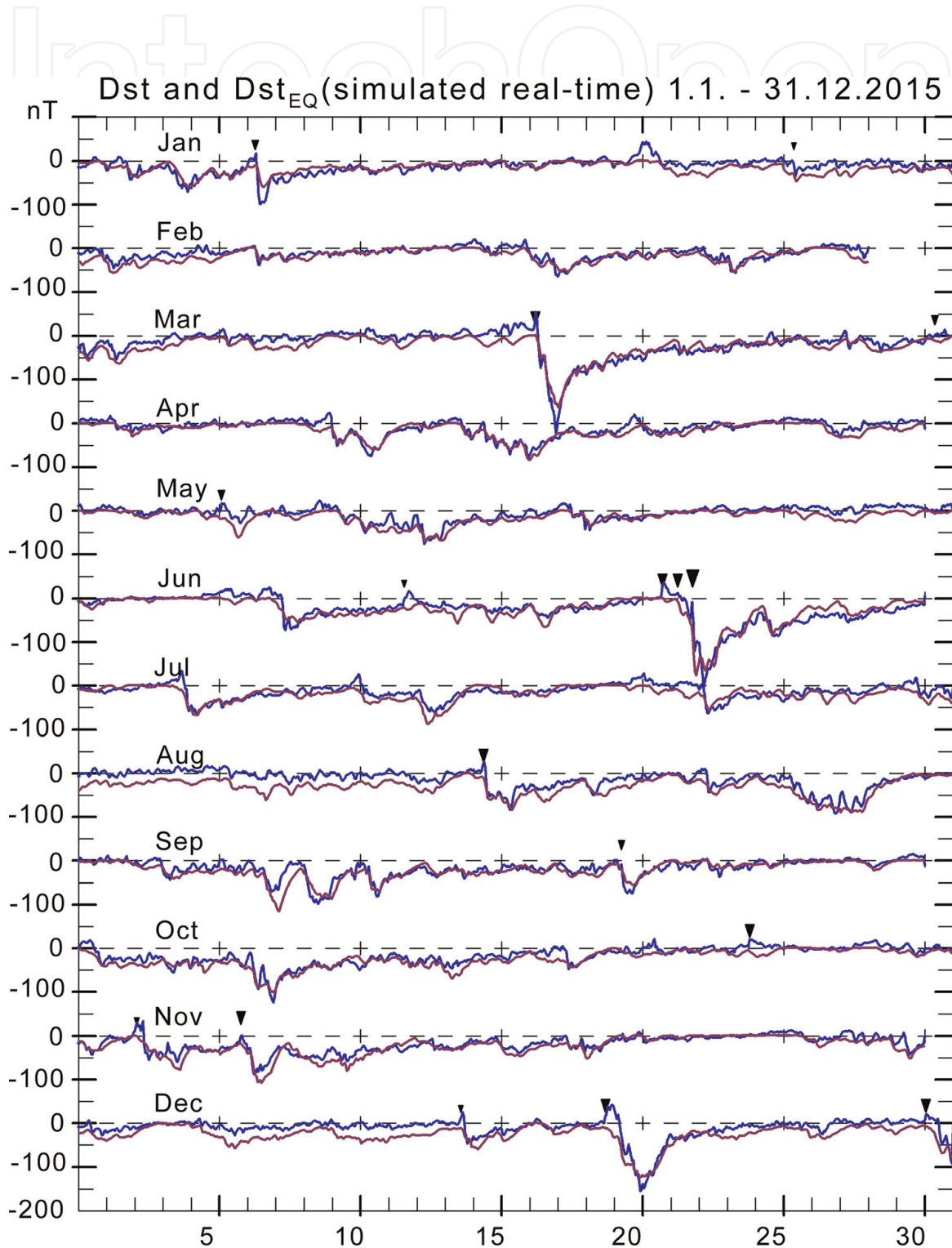
Figure 16.
Real (published) Dst values (blue line) and calculated PCC-based Dst_{EQ} values (magenta) in simulated real-time for 2015. Storm sudden commencement (SSC) events are displayed by the downward pointing black triangles to indicate onset times and sized to indicate their amplitudes [from [62]].

Thus, the use of real-time PCC indices will not change in any significant amount any of the relations between the polar cap indices and the magnetospheric current systems discussed in the present contribution mostly based on post-event analyses.

Using QDC values calculated in the real-time version, that is, from past days only with respect to current time, enables the calculation of PCN and PCS and, thus, PCC indices in simulated real-time versions. These versions have been used in the lengthy integration from 2009 to 2019 to calculate PCC-based equivalent Dst indices. An interim result for 2015 is displayed in **Figure 16** in the format of **Figure 14**.
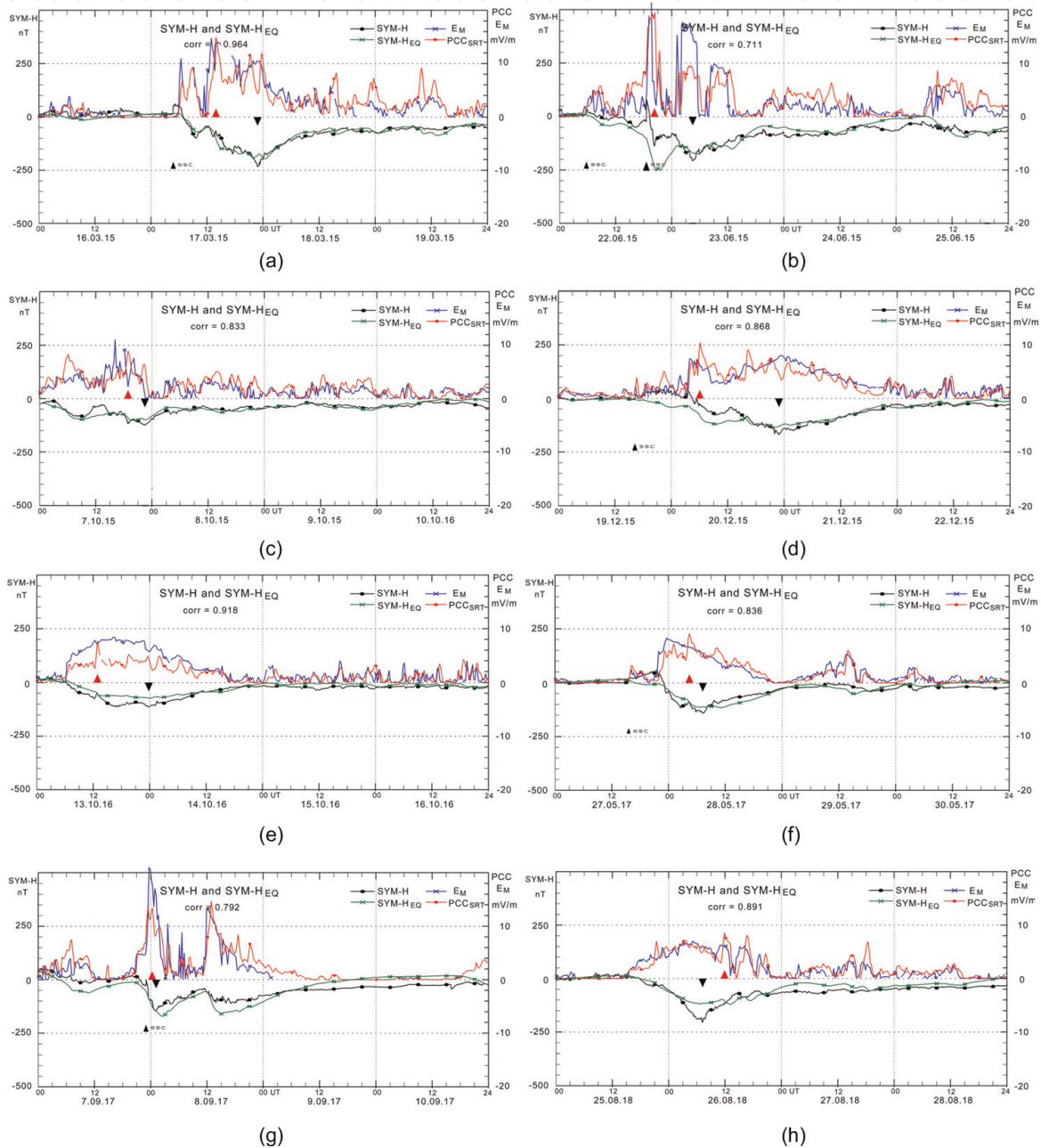
Figure 17.
(a–d) Examples of storm events. Low-latitude observations-based (real) SYM-H indices (black line with dots) and equivalent SYM-H$_{EQ}$ index values (green, crosses) calculated from the source function [Eq. (10)] using the PCC$_{SRT}$ values (red) shown in the upper fields along with merging electric field values, E$_M$, (blue), displayed on the right scale. Upward pointing red triangles at the mid-line indicate PCC maxima. Downward black triangles indicate SYM-H minima. The size and pointing of the small black triangles labeled SSC indicate intensity and onset time of storm sudden commencements [after [62]].

The match between the real and the simulated Dst values in the simulated real-time example shown in **Figure 16** is as good as seen in the corresponding post-event example displayed in **Figure 14**.

The use of simulated real-time calculations of SYM-H indices is illustrated in **Figure 17a–d** for a sequence of storm cases observed between March 2015 and June 2018. The diagrams present, in the lower fields, the values of SYM-H (black line with dots) and SYM-H$_{EQ}$ (green line). The upper fields of the diagrams in **Figure 17** present the PCC indices and, in addition, the values of the merging electric fields, E_M calculated from OMNIweb solar wind parameters (http://omniweb.gsfc.nasa.gov).

It the examples in **Figure 17**, there are several noteworthy features such as the close agreement between the real SYM-H values and equivalent SYM-H$_{EQ}$ values derived from PCC$_{SRT}$ indices calculated in simulated real-time using past values only in the calculations of QDC reference levels. The diagram presents the displays that would be seen in real-time space weather monitoring with access to polar magnetic data, space data to calculate E_M, and real SYM-H values in real time. The agreement between PCC and E_M values underlines their close correlation, as displayed in **Figures 3** and **4**. If space data for calculations of E_M and real SYM-H values are not available, then PCC and the PCC-based equivalent SYM-H values might provide worthwhile substitutes at space weather monitoring.

Note, in passing, the scatter in the relative occurrences of maxima in PCC and minima in SYM-H as depicted by the positions of the upward pointing red triangles and the downward pointing black triangles at the midline. This scatter is in strong contrast to the regularity in timing claimed by Troshichev and Sormakov [26] and included in the report ISO-TR/23989 from the International Organization for Standardization (ISO) [35].

In the publication and in the ISO report, they state that maximum depression (minimum SYM-H) would occur "*with typical delay time of ΔT = 1.5 ± 0.5 h*" after the peak in the PC index. This statement is obviously incorrect for all but one of the eight cases presented in **Figure 16** (six cases of ΔT = 4–14 h, 1 case of ΔT = –6 h). The invalid statements from Troshichev and Sormakov [26] included in the ISO [35] report could be seriously misleading at space weather monitoring when trusting that the ISO represents the supreme authority in space environment.

10. Discussions

10.1 PC index concept

Using the Kan and Lee [21] merging electric field (energy coupling function) for scaling of the index calibration parameters is a fundamental premise for the development of the present PC index concept [10]. However, it is quite possible that the reference energy coupling function could be improved. Further coupling functions, like those suggested by Lyatsky and Khazanov [63], Tenfjord and Østgaard [64], or McPherron et al. [65], might provide more precise relations between solar wind parameters and geomagnetic disturbances but at the cost of simplicity. The task of comparing the performances of different energy coupling functions awaits a dedicated initiative.

However, the results for the relations between polar cap indices and indices for further major magnetospheric current systems reported here strongly favor the present PC index concept expressed in Sections 2 and 3.

10.2 Correlation techniques

For the works reported in present manuscript, all the correlations were made by using a linear product-moment formula. Most regression calculations were made by applying linear least squares regression using the basic sample types considered most useful for the purpose. For the correlation and regression calculations for PC indices against solar wind parameters and global magnetic disturbance indices, 1-min data samples are available. However, the faster variations may not be transferred in complete details between the solar wind and the polar ionosphere or between the polar cap and the ring current regimes. Thus, for PC-E_M, PC-ASY-H, and PC-SYM-H relations, 15-min samples were used, while 5-min samples were used for the relations between the PC indices and the auroral electrojet intensities and for the onset conditions defined through the AL, AU, SML, and SMU indices. The PC index data were first converted from 1-min to 5-min averages by removing the max and min values for spike suppression. Next, 5-min or 15-min averages were formed from the remaining samples assuming that similar spike suppression measures have been applied to the other parameters by the index suppliers.

10.3 Forward versus reverse convection conditions

The present work discusses the statement in Resolution no. 3 [66], that International Association of Geomagnetism and Aeronomy (IAGA) is "*considering that the Polar Cap (PC) index constitutes a quantitative estimate of geomagnetic activity at polar latitudes and serves as a proxy for energy that enters into the magnetosphere during solar wind-magnetosphere coupling.*"

The first part of the statement is evident, while the second part is based on the close relation between the solar wind merging electric field parameter (E_M) and PC index values as well as the association between PC index levels and various energy dissipation processes, such as auroral activity and building ring currents [23–26, 35, 67–69]. However, the occurrences of negative PC index cases are usually ignored and left out in these associations, and the question on interpretation of negative index values remains open.

It is a fundamental issue for the polar cap index concept that the antisunward transpolar forward convection mode (DP2) at southward IMF is fundamentally different from the reverse convection mode (DP3) associated with northward IMF conditions. The differences appear in the correlation and regression relations between the non-negative values of the merging electric field [cf. Eq. (3)] and the projected magnetic variations that could have positive as well as negative (or even strongly negative) values. In the forward convection cases (positive PC indices), the disturbance level rises with increasing values of the merging electric field that controls the input of solar wind energy into the magnetosphere. In these cases, the PC indices track the merging electric field values. However, as the IMF turns northward (positive B_Z), the transpolar convection may turn sunward (reverse), whereby the PC indices may reach large negative values that could not possibly keep any proportionality with the decreasing but still positive merging electric field values. The examination of the relations in [29] has shown that reverse convection intensities amount to around 3% of the forward convection intensities for Vostok (PCS) and 10% for Qaanaaq (PCN) on the average. However, at daytime in the summer season, the relative amounts may rise to 6% for Vostok and up to 25% for Qaanaaq.

These differences between DP2 and DP3 cases were not implemented in the version [42] submitted jointly from AARI and DTU Space for endorsement by IAGA and

granted by its Resolution no. 3 [66]. When reverse convection cases are included, then the adverse effects on the calculations of scaling parameters cause, among others, uneven daily and seasonal relations between PC index values and values of E_M. The relative frequency of reverse convection cases is highest in the daytime hours of the summer season causing the adverse reducing effects on the PC-E_M correlation demonstrated in **Figures 3** and **4**.

The recognition of the differences between forward and reverse convection modes brought forward the PCC index concept Stauning [15] used extensively in the present contribution. These differences have also prompted the development of new calculation schemes for derivation of PCN and PCS scaling parameters (φ, α, and β), as reported in [14, 17, 70]. In the selection of samples from the epoch used for the calculation of PC index scaling parameters, cases of strong northward IMF (NBZ) conditions were omitted as far as possible.

In addition to differences in the calculation of PC index scaling parameters, the definition of the reference level, from which the magnetic disturbance values involved in calculations of the PC indices are measured (cf. Section 4), also differs between the IAGA-recommended PC index derivation methods [42, 71–74] and the SRW method [16] applied to derive reference levels ("QDC"s) for calculations of the indices considered here. These differences are elaborated in [20], where the problems are discussed. The main obstacle is the use of a solar wind sector term introduced by Janzhura and Troshichev [25] and used in the index calculations reported in [42] (see [20, 70, 75, 76]).

The good results from using PCC indices in auroral and ring current mapping reported here further support the concept of PCC indices being the optimum choice for estimates of solar wind energy input in post-event as well as in real-time applications. With the possibility of using data from Dome-C for useful PCS indices and Alert or Resolute Bay data for PCN indices [18, 19], the availability of useful PCC index series is greatly improved. Since 2009 and up to present (2022), there is hardly any interval without useful PCC index values. The present contribution has used data from all these sources with common unified derivation schemes. Comprehensive data and index quality control measures have been implemented throughout, among others, by comparing PC index values derived from different sources, thereby avoiding the invalid indices haunting the IAGA-endorsed PC index series [19, 20].

10.4 PC indices and the 1-min ring current indices

Building the ring currents flowing near equator at distances of 4–6 Earth radii (R_E) is usually considered a feature related to the amount of energy supplied from the solar wind to the magnetosphere [56–60]. For the asymmetrical ring current index, ASY-H, **Figure 10** displays a close relation between the average values of the polar cap PCC indices and the ASY-H indices all the way from near zero during quiet conditions to high values of both indices representing magnetic storm cases.

The direct relations between the SYM-H index and the PCC indices are inconclusive apart from indicating increased SYM-H values with increased PCC values (to be expected). Direct correlations between PC indices and SYM-H or Dst values beyond this trivial relation are not meaningful. This view is actually supported by the analysis of the relations between SYM-H and PC (here average of PCN and PCS) indices presented in [26]. Their **Figure 1** displays the level of correlation between SYM-H and PC indices with varying degree of smoothing of both parameters. The correlation coefficient increases steadily from 0.590 at 15-min samples through 0.625 at hourly

average samples to reach 0.657 (which may not be the maximum) at 120-min sample averaging. Thus, their correlation coefficient values, e.g., Rx = 0.625 at hourly average samples, agree well with the estimates in [29] of Rx = 0.623 (which is not maximum) for 15-min samples and 1-h shift and support the conclusion that the low-correlation coefficients indicate poor correspondence between simultaneous PC and Dst (or SYM-H) index values.

Guidance by the calculations presented by Burton et al. [58] has enabled the calculations of equivalent Dst index values based on using PC indices in the gradient source function and in the first step using the timing parameters from Feldstein et al. [59]. The iteration of control parameters to reach an optimal result for the equivalent Dst index depends on the quality parameter considered, whether being the coefficients of correlation with the published (real) Dst values or the mean and rms differences with respect to the equivalent (PC-based) Dst (or SYM-H) values. The relations also depend on the selection of samples considered. The Dst_{EQ} for moderate events would match the real Dst values closer than seen in the very strong or rather weak events. Thus, there is no unique set of "correct" control parameters. The set of values presented in the "optimum" column of **Table 3** is considered the best compromise.

10.5 The PC index as indicator of solar wind energy input

In IAGA Resolution #3 [66] as well as in many reported investigations, the solar wind merging electric field E_M (often named E_{KL}) derived from solar wind parameters at the front of the magnetosphere is considered to control the amount of solar wind energy that enters the magnetosphere. Thus, disregarding negative values, the polar cap indices, since they are scaled with respect to E_M, have been considered to represent the input of solar wind energy to the magnetosphere to power various geomagnetic disturbances such as polar magnetic variations, auroral activities, substorms, upper atmosphere heating, and the building of ring currents [10, 11, 23–25, 68, 77]. Such investigations were previously based on separate PCN or PCS indices, or on their plain averages, or on the summer/winter hemisphere PC index selections. Thus, the improved correlation with E_M resulting from using the PCC indices as reported here might improve results from such investigations.

Some of the relations between PC indices and geomagnetic disturbances could be described to a fair approximation by linear relations possibly with timing shifts to account for propagation delays or inertia effects. However, the gradual building of the symmetrical ring currents to represent energy input from the solar wind to the magnetosphere supports the concept of using the polar cap indices in a gradient source function rather than comparing the PC indices directly to the actual ring current indices. The development of the Dst ring current indices, in particular their

Correlation	PCC	PCN	PCS	PCA[1]	PCW[2]	PCU[3]
E_M	**0.770**	0.708	0.725	0.755	0.738	0.697
ASY-H[4]	**0.743**	0.702	0.679	0.716	0.700	0.683

[1]*Average of PCN and PCS.*
[2]*Selection of winter hemisphere PC indices.*
[3]*Selection of summer hemisphere PC indices.*
[4]*Magnetic storm events (1992–2018).*

Table 5.
Correlation coefficients for epoch 1998–2018 [from [29]].

(negative) peak values, relates to the intensity-time history of the PC indices and not to any specific instantaneous value.

10.6 Quality control

All the aspects of the investigations of the relations between the polar cap indices and the merging electric field and the ring current properties rely critically on the quality of the basic magnetic data and their proper handling. Thus, with profound respect for such concerns, all magnetic observational data involved here have been inspected in plots like the diagrams displayed in **Figure 1a** and **b** of monthly and yearly averages for international quiet (QQ) days. The component base lines have been controlled and—if needed—corrected to provide smooth secular variations only. The QDC values needed for defining the magnetic variations have also been displayed in yearly summary plots corresponding to the samples presented here in **Figure 2a** and **b** or in **Figure 9** of Stauning [16] defining the solar rotation weighting (SRW) QDC method or the PC index reports [14, 17]. The PC indices have been inspected in monthly plots similar to the samples presented in Stauning et al. [14] or Stauning [17]. In addition, the derived equivalent Dst indices (Dst_{EQ}) have been displayed along with the published Dst indices for each of the storm cases in the formats of **Figures 14** and **16**. Diagrams for the entire integration interval from 1992 to 2018 are included in Appendix A of [29]. It appears that corresponding quality measures have not been considered for the IAGA-endorsed indices [20].

11. Summary

11.1 Relations between the merging electric fields and PC indices

The examinations of the relations between the solar wind merging electric field, E_M, and the polar cap indices, PCN, PCS, and PCC, presented in **Figures 3** and **4** have demonstrated, unambiguously, that the non-negative combined PCC indices present higher values of the correlation with E_M than either of the PCN and PCS indices, their averages (PCA), or the seasonal selections, PCW for the local winter, and PCU for the summer index values throughout all years of available data and throughout all seasons of the years. A summary of correlation coefficients is shown in **Table 5**. On top of the PCC-E_M correlation with Rx = 0.770 shown in **Table 5**, the PCCD-E_M correlation (using Dome-C for questionable Vostok data) provides Rx = 0.786, the best score of all PC index combinations.

The examinations have also shown that the correlations between E_M and PCN or PCS have considerable seasonal variations with minima at local summer conditions, as displayed particularly clear in **Figure 4**. These minima are probably related in part to the corresponding maxima in the intensities of reverse convection (DP3) events. The seasonal variations have been mitigated in the PCC index version leaving a weak minimum at northern winter conditions (cf. **Figure 4**).

11.2 Relations between auroral activity and PC indices

The high, albeit seasonally varying, correlation coefficients and the regression slopes displayed in **Figure 7** provide a useful reference for the relations between polar cap and the auroral current systems. The rather broad range of PC index values

(0.25–2.25 mV/m) preceding substorms with onset steps of –100, –200, or –300 nT displayed in **Figure 9** indicates that the PC indices are not so useful in prediction of relatively weak substorm events. There is a particular problem with negative PCN and PCS index values since substorms are known to occur during strong NBZ conditions too. On the other hand, **Figure 9** also demonstrates that larger PC index levels of 2–4 mV/m are needed to generate the violent substorms with step amplitudes beyond 300 nT, which are those of particular relevance for space weather applications such as the prediction of GIC events threatening power grids [32, 33] rather than the hundreds of small substorms occurring every year.

11.3 Relations between ring current and polar cap indices

Fine-tuning of the control parameters and including modifications of the PCC indices for high-level saturation effects [cf. **Table 3** and Eqs. (13) and (14)] were used to calculate equivalent Dst_{EQ} indices by the integration of the source function [Eq. (10)] throughout the entire interval from 1992 to 2018 without any attachment to the real Dst index series. The correlation between the equivalent Dst index series using the source function based on the PCC indices derived from transpolar convection intensities and the real Dst indices based on near-equatorial magnetic observations reached a value of 0.856 at a delay of 45 min (PCC leading). The mean difference between the two series was below 1 nT, the mean absolute difference was below 10 nT, while the RMS difference was less than 13 nT (cf. **Table 4**).

In a simplified version of the small contributions ($\approx$20 nT) from the magnetopause currents, the Dst (or SYM-H) indices could be derived by integration (summations in small steps) of the rate of change defined by Eq. (10) using the parameters from **Table 3** and Eqs. (13) and (14) to provide the relation shown as follows [from [29]]:

$$d(Dst^*)/dt = gradD \cdot PCCeff - Dst^*/\tau \tag{15}$$

where

$$Dst* = Dst - 20 \text{ nT}$$

$$gradD = -4.5 \text{ (nT/h)/(mV/m)}$$

$$PCCeff = PCC \text{ if } PCC < 5 \text{ mV/m or } PCCeff = PCC + 0.6 \cdot (PCC - 5) \text{ if } PCC > 5 \text{ mV/m}$$

$$\tau = 5.5 \text{ h if } Dst < -52 \text{ nT or } \tau = 7.0 \text{ h if } Dst > -52 \text{ nT.}$$

Contrary to statements in [25, 26, 35], the present work (cf. **Figure 12**) has no indication of particular thresholds in the PC indices for ring current increases or decays. The ring currents monitored through the Dst_{EQ} (or $SYM\text{-}H_{EQ}$) indices start increasing as the PCC indices rise to a positive level, develops with the integrated time history of PCC, as shown, for instance, in Figures (13) and (14), and decays when the PCC-based source function in Eq. (10) [Eq. (10)] turns positive. There are no specific relations between the amplitude ratios or timing of PC maxima and Dst (or SYM-H) minima. The integration of Eq. (10) starting from quiet conditions (Dst $\approx$ 0) provides equivalent Dst (or SYM-H) index values up to $\approx$45 min ahead of actual time. Real-time PCC-based Dst index gradient source values provide the actual equivalent Dst (or SYM-H) forward slopes providing reliable ring current estimates at least 1 h ahead helping to decide whether storm conditions are intensifying or decaying.

12. Conclusions

- The present work has provided a systematic assessment of the correlation between various PC index versions used in published works with the merging electric field, E_M, in the solar wind and with ground-based global magnetic indices such as the auroral electrojet indices, AL, AU, SML, SMU, and the ring current indices, ASY-H, SYM-H, and Dst.

- The relations between the polar cap PCC indices, built from non-negative values of the PCN and PCS indices, and the solar wind merging electric field, E_M, are closer with markedly larger correlation coefficients than those found for the relations between E_M and either of the individual PCN or PCS indices, their averages, or the summer or winter hemisphere PC index selections throughout all years and regardless of the season.

- The correlation between the PCC indices and the auroral electrojet indices, AL and AU (or SuperMag SML and SMU), is so high that meaningful equivalent auroral indices could be derived to supplement or eventually replace the real indices at space weather monitoring.

- Substorm onset conditions relate closely to the PCC index level, particularly at the strong events endangering power grids through their GIC effects.

- For the scaling or forecasting of global disturbance conditions, the development of the asymmetric ring currents related to substorm activity could be monitored from the equivalent PC-based ASY-H index values, which are particularly useful, if the real index values are not available. For such applications, PCC indices rather than either of the hemispherical PC indices or other possible PC index combinations should be used to provide accurate and timely indications.

- The direct correspondence between the instantaneous PC index values and ring current Dst or SYM-H index levels or peak values is poor.

- The PC indices relate to the gradients (rate of change) in the symmetric ring current intensities monitored by the Dst or SYM-H indices. Accurate and detailed equivalent Dst_{EQ} or $SYM\text{-}H_{EQ}$ values could be derived to replace or supplement the real ring current indices and provide reliable forecasts of the symmetric ring currents up to 1 h ahead of actual time by the integration of the PCC-based source function from any previous known state.

- The close correspondence between real Dst and equivalent Dst index values at the integration throughout 1992–2018 providing correlation Rx = 0.86, mean deviation below 1 nT, and standard deviation less than 13 nT supports the concept of using PCC indices in a Dst_{EQ} source function. The accurate relations between the PCC-based Dst_{EQ} and the real Dst indices have enabled fine-tuning of timing parameters used in models of the ring current and has supported the modification of the PCC index values to counteract saturation effects at high disturbance levels.

- The high correlation and the accurate timing observed in the relations between the PCC indices based on transpolar convection of plasma and embedded

magnetic fields and the ring current indices derived from near-equatorial magnetic variations may provide new insight in and improved modeling of the physical processes linking the polar and equatorial geomagnetic disturbance phenomena and help resolving their common origin in the solar wind properties.

• The PC indices provide a great potential for space weather services by enabling monitoring of the input of solar wind energy to the magnetosphere where the energy is used to power disturbance processes such as polar and auroral activity, upper atmosphere heating, substorms, and geomagnetic storms. The PC indices enabling the input energy monitoring are derived from magnetic variations recorded at two oppositely located polar cap observatories only. The PCC indices improve the accuracy over other PC index versions. Using multiple sources for PCN and PCS indices would greatly improve service reliability.

Acknowledgements

Data availability

Geomagnetic data from Qaanaaq, Vostok, and Dome-C observatories were downloaded from the INTERMAGNET data service web portal at http://intermagnet.org. Ring current indices, Dst, SYM-H, and ASY-H, were downloaded from the web portal for World Data Centre WDC-C2 in Kyoto at http://swdcwww.kugi.kyoto-u.ac.jp/dstdir/index.html. Spacecraft data needed to generate the merging electric field values were downloaded from the OMNIweb service portal http://omniweb.gsfc.nasa.gov. SSC and QD data were downloaded from the ISGI data service portal http://isgi.unistra.fr. The SuperMag indices were downloaded from the web service at http://supermag.jhuapl.edu.

The magnetic observatory in Qaanaaq is managed by the Danish Meteorological Institute, while the magnetometer instruments are operated by DTU Space, Denmark. The Vostok observatory is operated by the Arctic and Antarctic Research Institute in St. Petersburg, Russia. The Dome-C observatory is managed by Ecole et Observatoire des Sciences de la Terre (France) and Istituto Nazionale di Geofisica e Vulcanologia (Italy).

The "DMI" PC index version is documented in the report SR-16-22 [17] available at the web site: http://www.dmi.dk/fileadmin/user_upload/Rapporter/TR/2016/SR-16-22-PCindex.pdf.

Keypoints

1. Demonstration of close relations between solar wind parameters, polar cap (PC) indices, and major magnetospheric current systems

2. Specification of relations between polar cap (PC), auroral (AL, AU and SML, SMU), and ring current (Dst, SYM-H, ASY-H) indices.

3. Development of methods for the application of real-time polar cap (PC) indices in space weather monitoring.

Author details

Peter Stauning
Danish Meteorological Institute, Copenhagen, Denmark

*Address all correspondence to: pst@dmi.dk

IntechOpen

References

[1] Dungey JW. Interplanetary magnetic field and the auroral zones. Physical Review Letters. 1961;**6**:47-48. DOI: 10.1103/PhysRevLett.6.47

[2] Obayashi T. The interaction of solar plasma with geomagnetic field, disturbed conditions. In: King JW, Newman WS. Solar Terrestrial Physics. Academic Press, New York; 1967. p. 107

[3] Nishida A. Geomagnetic Dp 2 fluctuations and associated magnetospheric phenomena. Journal of Geophysical Research. 1968;**73**(5): 1795-1803. DOI: 10.1029/JA073i005 p01795

[4] Nishida A, Maezawa K. Two basic modes of interaction between the solar wind and the magnetosphere. Journal of Geophysical Research. 1971;**76**:2254

[5] Dungey, JW. The structure of the exosphere or adventures in velocity space, in: Geophysics, The Earth's Environment. In: DeWitt C, Hieblot J, LeBeau L, pp. 503–550, Gordon and Breach, New York. 1963.

[6] Lockwood M, McWilliams KA. A survey of 25 years' transpolar voltage data from the SuperDARN radar network and the expandingcontracting polar cap model. Journal of Geophysical Research: Space Physics. 2021;**126**: e2021JA029554. DOI: 10.1029/ 2021JA029554

[7] Fairfield DH. Polar magnetic disturbances and the interplanetary magnetic field. COSPAR Space Research. 1968;**VIII**:107. DOI: 10.1029/ JZ071i001p00155

[8] Kuznetsov BM, Troshichev OA. On the nature of polar cap magnetic activity during undisturbed periods. Planetary

and Space Science. 1977;**25**:15-21. DOI: 10.1016/0032-0633(77)90113-1

[9] Troshichev OA, Andrezen VG. The relationship between interplanetary quantities and magnetic activity in the southern polar cap. Journal of Planetary and Space Science. 1985;**33**:415-419. DOI: 10.1016/0032-0633(85)90086-8

[10] Troshichev OA, Andrezen VG, Vennerstrøm S, Friis-Christensen E. Magnetic activity in the polar cap–A new index. Journal of Planetary and Space Science. 1988;**36**(11):1095-1102. DOI: 10.1016/0032-0633(88)90063-3

[11] Vennerstrøm S, Friis-Christensen E, Troshichev OA, Andrezen VG. Comparison between the polar cap index PC and the auroral electrojet indices AE, AL and AU. Journal of Geophysical Research: Space Physics. 1991;**96**(A1): 101-113. DOI: 10.1029/90JA01975

[12] Troshichev OA, Janzhura AS, Stauning P. Unified PCN and PCS indices: Method of calculation, physical sense and dependence on the IMF azimuthal and northward components. Journal of Geophysical Research. 2006; **111**:A05208. DOI: 10.1029/ 2005JA011402 Note correction in Troshichev et al. [13]

[13] Troshichev OA, Janzhura AS, Stauning P. Correction to "Unified PCN and PCS indices: Method of calculation, physical sense, and dependence on the IMF azimuthal and northward components". Journal of Geophysical Research. 2009;**114**:A11202. DOI: 10.1029/2009JA014937

[14] Stauning P, Troshichev OA, Janzhura A. Polar cap (PC) index. Unified PC-N (North) index procedures

and quality. DMI Scientific Report, SR-06-04. 2006. Available from: https://www.dmi.dk/fileadmin/Rapporter/SR/sr06-04.pdf

[15] Stauning P. A new index for the interplanetary merging electric field and geomagnetic activity: Application of the unified polar cap indices. Space Weather. 2007;**5**:S09001. DOI: 10.1029/2007SW000311

[16] Stauning P. Determination of the quiet daily geomagnetic variations for polar regions. Journal of Atmospheric and Solar-Terrestrial Physics. 2011;**73**:2314-2330. DOI: 10.1016/j.jastp.2011.07.004

[17] Stauning P. The polar cap (PC) index: Derivation procedures and quality control. DMI Scientific Report SR-16-22. 2016. Available from: https://www.dmi.dk/fileadmin/user_upload/Rapporter/TR/2016/SR-16-22-PCindex.pdf

[18] Stauning P. Multi-station basis for polar cap (PC) indices: Ensuring credibility and operational reliability. Journal of Space Weather and Space Climate. 2018;**8**:A07. DOI: 10.1051/swsc/2017036

[19] Stauning P. Reliable polar cap (PC) indices for space weather monitoring and forecast. Journal of Space Weather and Space Climate. 2018;**8**:A49. DOI: 10.1051/swsc/2018031

[20] Stauning P. The polar cap (PC) index: Invalid index series and a different approach. Space Weather. 2020;**18**(10):1-18. DOI: 10.1029/2020SW002442 (accepted for publication)

[21] Kan JR, Lee LC. Energy coupling function and solar wind-magnetosphere dynamo. Geophysical Research Letters. 1979;**6**(7):577-580. DOI: 10.1029/GL006i007p00577

[22] Milan SE, Carter JA, Sangha H, Bower GE, Anderson BJ. Magnetospheric flux throughput in the Dungey cycle: Identification of convection state during 2010. Journal of Geophysical Research: Space Physics. 2021;**126**:e2020JA028437. DOI: 10.1029/2020JA028437

[23] Janzhura AS, Troshichev OA, Stauning P. Unified PC indices: Relation to the isolated magnetic substorms. Journal of Geophysical Research. 2007;**112**:A09207. DOI: 10.1029/2006JA012132

[24] Troshichev OA, Podorozhkina NA, Sormakov DA, Janzhura AS. PC index as a proxy of the solar wind energy that entered into the magnetosphere: 1. Development of magnetic substorms. Journal of Geophysical Research: Space Physics. 2014;**119**:6521. DOI: 10.1002/2014JA019940

[25] Troshichev OA, Sormakov DA, Janzhura AS. Relation of PC index to the geomagnetic storm Dst variation. Journal of Atmospheric and Solar-Terrestrial Physics. 2011;**73**:611-622. DOI: 10.1016/j.jastp.2010.12.015

[26] Troshichev OA, Sormakov DA. PC index as a proxy of the solar wind energy that entered into the magnetosphere: (3) Development of magnetic storms. Journal of Atmospheric and Solar-Terrestrial Physics. 2018;**180**:60-77. DOI: 10.1016/j.jastp.2017.10.012

[27] Stauning P, Troshichev OA, Janzhura AS. The polar cap (PC) index: Relations to solar wind parameters and global activity level. Journal of Atmospheric and Solar-Terrestrial Physics. 2008;**70**:2246-2261. DOI: 10.1016/j.jastp.2008.09.028

[28] Stauning P. The polar cap PC indices: Relations to solar wind and global disturbances. In: Lazar M, editor.

Exploring the Solar Wind. London ISBN: 978-953-51-0339-4: IntechOpen; 2012. DOI: 10.5772/37359

[29] Stauning P. The polar cap (PC) index combination, PCC: Relations to solar wind properties and global magnetic disturbances. Journal of Space Weather and Space Climate. 2021;**11**(19):1-23. DOI: 10.1051/swsc/2020074

[30] Kappenman J. Geomagnetic storms and their impact on the U.S. power grid. Metatech Report, Meta-R-319. 2010. 197 pp. Available from: https://www.ferc.g ov/sites/default/files/2020-05/ferc_me ta-r-319.pdf

[31] Pulkkinen A, Bernabeu E, Thomson A, et al. Geomagnetically induced currents: Science, engineering, and applications readiness. Space Weather. 2017;**15**:828-856. DOI: 10.1002/ 2016SW001501

[32] Stauning P. Power grid disturbances and polar cap index during geomagnetic storms. Journal of Space Weather and Space Climate. 2013;**3**:A22. DOI: 10.1051/swsc/2013044

[33] Stauning P. Using PC indices to predict violent GIC events threatening power grids. Journal of Space Weather and Space Climate. 2020;**10**(3):1-13. DOI: 10.1051/swsc/2020004

[34] Roeder JL, Jordanova VK. Space weather effects and prediction, Ch. 8. In: Jordanova JK, Ilie R, Chen MW, editors. Ring Current Investigations. Elsevier; 2020. pp. 153-244, ISBN: 978-0-12-815571-4. DOI: 10.1016/B978-0-12-815571-4.00008-1

[35] Space environment (natural and artificial)—Operational estimation of the solar wind energy input into the Earth's magnetosphere by means of the ground-based polar cap (PC) index. ISO Report.

International Organization for Standardization. ISO Technical Report ISO/TR/23989-2020. 2020. Available from: https://www.iso.org/standard/ 77565.html

[36] Akasofu S-I. The development of the auroral substorm. Planetary and Space Science. 1964;**12**(4):273-282. DOI: 10.1016/0032-0633(64)90151-5

[37] Akasofu S-I. Physics of Magnetospheric Substorms. Dordrecht-Holland: D. Reidel Publ. Co.; 1977. pp. 190-220

[38] Akasofu S-I. Interplanetary energy flux associated with magnetospheric substorms. Planetary and Space Science. 1979;**27**:425

[39] Chambodut A, Di Mauro D, Schott JJ, Bordais P, Agnoletto L, Di Felice P. Three years continous record of the Earth's magnetic field at Concordia station (Dome-C, Antarctica). Annals of Geophysics. 2009;**52**:15-24. DOI: 10.4401/ag-4569

[40] Di Mauro D, Cafarella L, Lepidi S, Pietrolungo M, Alfonsi L, Chambodut A. Geomagnetic polar observatories: The role of Concordia station at Dome C, Antartica. Annals of Geophysics. 2014;**57** (6):G0656. DOI: 10.4401/ag-6605

[41] Vennerstrøm S. The geomagnetic activity index PC [PhD thesis]. DMI Scientific Report 91-3. Danish Meteorological Institute; 1991. 105 pp. Available from: https://www.dmi.dk/f ileadmin/user_upload/Rapporter/SR/ 1991/sr91-3.pdf

[42] Matzka J, Troshichev OA. PC_index_ description_main_document_incl_ Appendix_A.pdf. 2014. Available from: DTU Space web portal. doi:10.11581/ DTU:00000057

[43] Janzhura AS, Troshichev OA. Determination of the running quiet daily geomagnetic variation. Journal of Atmospheric and Solar-Terrestrial Physics. 2008;**70**:962-972. DOI: 10.1016/j.jastp.2007.11.004

[44] Akasofu S-I. Relationship between the AE and Dst indices during geomagnetic storms. Journal of Geophysical Research. 1981;**86**:4820-4822

[45] Iijima T, Potemra TA. The amplitude distribution of field-aligned currents at northern high latitudes observed by Triad. Journal of Geophysical Research. 1976;**81**:2165-2174

[46] Iijima T, Potemra TA. Field-aligned currents in the day-side cusp observed by Triad. Journal of Geophysical Research. 1976;**81**:5971-5979

[47] Bythrow PF, Potemra TA. The relationship of total Birkeland currents to the merging electric field. Geophysical Research Letters. 1983;**10**:573-576

[48] Gjerloev JW, Hoffman RA. The large-scale current system during auroral substorms. Journal of Geophysical Research: Space Physics. 2014;**119**:4591-4606. DOI: 10.1002/2013JA019176

[49] McPherron RL, Russell C, Aubry M. 9. Phenomenological model for substorms. Journal of Geophysical Research. 1973;**78**(16):3131-3149. DOI: 10.1029/JA078i016p03131

[50] Davis TN, Sugiura M. Auroral electrojet activity index AE and its Universal Time variations. Journal of Geophysical Research. 1966;**71**:785-801. DOI: 10.1029/JZ071i003p00785

[51] Iyemori T, Araki T, Kamei T, Takeda M. Mid-latitude geomagnetic indices "ASY" and "SYM" for 1999, Geomagnetic indices home page. In: Iyemori T, editor. WDC-C2 for Geomagnetism. Kyoto, Japan: Kyoto University. 2000. Available from: http://swdcwww.kugi.kyoto-u.ac.jp/dstdir/index.html

[52] Gjerloev JW. The SuperMAG data processing technique. Journal of Geophysical Research. 2012;**117**:A09213. DOI: 10.1029/2012JA017683

[53] McPherron RL, Chu X. The midlatitude positive bay index and the statistics of substorm occurrence. Journal of Geophysical Research: Space Physics. 2018;**123**(4):2831-2850. DOI: 10.1002/2017JA024766

[54] Sugiura M, Kamei T. Description of the hourly Dst index. In: Iyemori T, editor. Geomagnetic Indices Home Page. WDC-C2 for Geomagnetism. Kyoto, Japan: Kyoto University; 1981. Available from: http://swdcwww.kugi.kyoto-u.ac.jp/dstdir/index.html

[55] Bartels J. The geomagnetic measures for the time variations of solar corpuscular radiation, described for use in correlation studies in other geophysical fields. Ann Intern Geophys Year. 1957;**4**:227-236

[56] Dessler AJ, Parker EN. Hydromagnetic theory of geomagnetic storms. Journal of Geophysical Research. 1959;**64**:2239-2259. DOI: 10.1029/JZ064i012p02239

[57] Sckopke N. A general relation between the energy of trapped particles and the disturbance field near the Earth. Journal of Geophysical Research. 1966;**71**:3125-3130. DOI: 10.1029/JZ071i013p03125

[58] Burton RK, McPherron RL, Russell CT. An empirical relationship between interplanetary conditions and Dst. Journal of Geophysical Research. 1975;

80:4204-4214. DOI: 10.1029/JA080i 031p04204

[59] Feldstein YI, Pisarsky VY, Rudneva NM, Grafe A. Ring current simulation in connection with interplanetary space conditions. Planetary and Space Science. 1984;**32**:975-984. DOI: 10.1016/0032-0633(84)90054-0

[60] Jorgensen AM, Spence HE, Hughes WJ, Singer HJ. A statistical study of the ring current. Journal of Geophysical Research. 2004;**109**:A12204. DOI: 10.1029/2003JA010090

[61] Gao Y. On anomalous departures from a linear relation between the polar cap index and its controlling factors in the solar wind and magnetotail. Journal of Geophysical Research. 2012;**117**: A06201:1-A06201:10. DOI: 10.1029/ 2012JA017721

[62] Stauning P. Transpolar convection and magnetospheric ring currents: Real-time applications of polar cap (PC) indices. Space Weather. 2021;**19**(7):1-25. DOI: 10.1029/2020SW002072

[63] Lyatsky W, Khazanov GV. A new polar magnetic index of geomagnetic activity. Space Weather. 2008;**6**: S06002. DOI: 10.1029/2008SW 000382

[64] Tenfjord P, Østgaard N. Energy transfer and flow in the solar wind-magnetosphere–ionosphere system. A new coupling function. Journal of Geophysical Research: Space Physics. 2013;**118**:5659-5672. DOI: 10.1002/ jgra50545

[65] McPherron RL, Hsu T-S, Chu X. An optimum solar wind coupling function for the AL index. Journal of Geophysical Research: Space Physics. 2015; **120**(4):2494-2515. DOI: 10.1002/ 2014ja020619

[66] IAGA Resolution No. 3. 2013. Available from: http://www.iaga-aiga. org/resolutions

[67] Troshichev OA, Janzhura AS. Space Weather Monitoring by Ground-Based Means. Heidelberg: Springer Praxis Books; 2012. DOI: 10.1007/978-3-642-16803-1

[68] Troshichev OA, Sormakov DA. PC index as a proxy of the solar wind energy that entered into the magnetosphere: (2) Relation to the interplanetary electric field E_{KL}. Earth, Planets and Space. 2015; **67**:170. DOI: 10.1186/s40623-015-0338-4

[69] Troshichev OA, Sormakov DA. PC index as a proxy of the solar wind energy that entered into the magnetosphere: (5) Verification of the solar wind parameters presented at OMNI website. Journal of Atmospheric and Solar-Terrestrial Physics. 2019;**196**:105-147. DOI: 10.1016/j.jastp.2019.105147

[70] Stauning P. The polar cap index: A critical review of methods and a new approach. Journal of Geophysical Research: Space Physics. 2013;**118**:5021-5038. DOI: 10.1002/jgra.50462

[71] Janzhura AS, Troshichev OA. Identification of the IMF sector structure in near-real time by ground magnetic data. Annales Geophysicae. 2011;**29**:1491-1500. DOI: 10.5194/angeo-29-1491-2011

[72] Nielsen JB, Willer AN. Restructuring and harmonizing the code used to calculate the Definitive Polar Cap Index. Report from DTU Space. 2019. Available from: https://tinyurl.com/sx3g5t5

[73] Troshichev OA. Polar cap (PC) index. 2011. Available from: http:// pcindex.org (see Supported materials)

[74] Troshichev OA. Polar cap magnetic activity (PC index) and space weather

monitoring. Édition Universitaires Européennes. 2017. ISBN: 978-3-8381-8012-0

[75] Stauning P. Comments on quiet daily variation derivation in "Identification of the IMF sector structure in near-real time by ground magnetic data" by Janzhura and Troshichev (2011). Annales de Geophysique. 2013;**31**:1221-1225. DOI: 10.5194/angeo-31-1221-2013

[76] Stauning P. A critical note on the IAGA-endorsed polar cap index procedure: Effects of solar wind sector structure and reverse polar convection. Annales de Geophysique. 2015;**33**:1443-1455. DOI: 10.5194/angeo-33-1443-2015

[77] Troshichev AO, Lukianova RY. Relation of PC index to the solar wind parameters and substorm activity in time of magnetic storms. Journal of Atmospheric and Solar - Terrestrial Physics. 2002;**64**:585. DOI: 10.1016/S1364-6826(02)00016-0